

Regulation of the Protocadherin *Celsr3* Gene and Its Role in Globus Pallidus Development and Connectivity

Zhilian Jia,^{a,b,c} Ya Guo,^{a,b,c} Yuanxiao Tang,^{a,b,c} Quan Xu,^{a,b,c} Baojie Li,^c Qiang Wu^{a,b,c}

Key Laboratory of Systems Biomedicine (Ministry of Education), Center for Comparative Biomedicine, Institute of Systems Biomedicine, Shanghai Jiao Tong University, Shanghai, China^a; State Key Laboratory of Oncogenes and Related Genes, Shanghai Cancer Institute, Renji Hospital, School of Medicine, Shanghai Jiao Tong University, Shanghai, China^b; Key Laboratory for the Genetics of Developmental and Neuropsychiatric Disorders, Ministry of Education, Bio-X Center, School of Life Sciences and Biotechnology, Shanghai Jiao Tong University, Shanghai, China^c

The globus pallidus (GP) is a central component of basal ganglia whose malfunctions cause a variety of neuropsychiatric disorders as well as cognitive impairments in neurodegenerative diseases such as Parkinson's disease. Here we report that the protocadherin gene *Celsr3* is regulated by the insulator CCCTC-binding factor (CTCF) and the repressor neuron-restrictive silencer factor (NRSF, also known as REST) and is required for the development and connectivity of GP. Specifically, CTCF/cohesin and NRSF inhibit the expression of *Celsr3* through specific binding to its promoter. In addition, we found that the *Celsr3* promoter interacts with CTCF/cohesin-occupied neighboring promoters. In *Celsr3* knockout mice, we found that the ventral GP is occupied by aberrant calbindin-positive cholinergic neurons ectopic from the nucleus basalis of Meynert. Furthermore, the guidepost cells for thalamocortical axonal development are missing in the caudal GP. Finally, axonal connections of GP with striatum, subthalamic nucleus, substantia nigra, and raphe are compromised. These data reveal the essential role of *Celsr3* in GP development in the basal forebrain and shed light on the mechanisms of the axonal defects caused by the *Celsr3* deletion.

The genes *Celsr1*, *Celsr2*, and *Celsr3* are members of the mammalian nonclustered protocadherin (*Pcdh*) family that are homologous to the fly *flamingo* gene (1). The *flamingo* gene plays important roles in dendrite development and self-avoidance, axonal projection, and planar cell polarity (PCP) in *Drosophila* (2–7). The mammalian *Celsr* genes are the so-called core PCP genes that have conserved as well as newly diversified functions. In particular, the vertebrate *Celsr3* gene has been shown to regulate axonal projections, dendrite development, neuronal migration, cilogenesis, and retina circuit development (8–16). However, very little is known about *Celsr* gene regulation.

The globus pallidus (GP) is a central nucleus of the basal ganglia (BG) (17, 18). Malfunctions of GP lead to several neuropathological conditions, such as Parkinson's disease, as well as many neuropsychiatric diseases (19). The mouse GP, which corresponds to the GPe in primates, contains approximately 44% of parvalbumin-positive (PV⁺) neurons and 1% of calretinin-positive (CR⁺) interneurons, but calbindin-positive (CB⁺) cells are rare (20, 21). The GP is traditionally thought to be derived from the medial ganglionic eminence (MGE) (22); however, recent studies have revealed that, in addition to MGE, subpopulations of GP cells are also generated from the lateral ganglionic eminence (LGE) and preoptic area (POA) (21, 23). The molecular requirements for GP development are not known, but specific transcription factors appear to be essential. For example, *Nkx2-1* is required for the generation of most GP neurons except the Npas1⁺ type from LGE (23). In addition, *Lhx6/8* double-mutant mice do not have a well-defined GP (24).

The GP functions through extensive axonal connections with other brain nuclei. For example, GP receives GABAergic axons from the striatum, glutamatergic fibers from the subthalamic nucleus (STN), dopaminergic axons from the substantia nigra pars compacta (SNc), and serotonergic axons from the raphe (18, 20). In turn, GP sends GABAergic fibers to the output nuclei: the entopeduncular nucleus (EP, or GPi in primates) and the STN

(18–20). Finally, the cells close to or associated with the developing GP might assist in the development of the major thalamocortical and corticofugal pathways as guidepost cells in the ventral forebrain (25–29). However, little is known about the molecular mechanisms of the development of GP connectivity.

We report that the transcription factors CCCTC-binding factor (CTCF) and neuron-restrictive silencer factor (NRSF) regulate the expression of *Celsr3* by directly binding to its promoter region. In particular, the *Celsr3* promoter interacts with several other promoters, most of which are enriched with the histone mark H3K4me3 and CTCF/cohesin, through long-distance DNA looping. In addition, we report the critical role of *Celsr3* in GP development and connectivity. Specifically, we have found that the ventral region of the *Celsr3* mutant GP is occupied by cholinergic neurons ectopic from the nucleus basalis of Meynert (NB) and that the axonal connections of the GP with other nuclei are compromised. Taken together, these data suggest that *Celsr3*, regulated by CTCF/cohesin and NRSF, is essential for GP development and connectivity.

MATERIALS AND METHODS

Plasmid construction. The sequences for the mouse full-length *Celsr3* open reading frame (ORF) (9,930 bp) were cloned from brain total RNA preparations by reverse transcriptase PCR (RT-PCR) experiments. We first designed four pairs of primers (F1, AGTAG ATGGT GCCCA GAGAG CAGTG; R1, GTGCT GATGG CAAAT CGGTT CCGAG; F2, ACAGC GCCAT CAGCT ACCAA ATCAC; R2, CGTTG CAGTC ATCCA

Received 3 June 2014 Returned for modification 9 July 2014

Accepted 1 August 2014

Published ahead of print 11 August 2014

Address correspondence to Qiang Wu, qwu123@gmail.com.

Copyright © 2014, American Society for Microbiology. All Rights Reserved.

doi:10.1128/MCB.00760-14

CGCTC AACAC; F3, CAGGA GGCCT GAGTG ACGGA CAATG; R3, GCTGG CCTTG TTTCC TCAGG AGCTG; F4, TTGGA CACCA GCCTG TCTAG GCAAG; R4, AGGAG TGACC CTCGC TTCTG GGAAC) to amplify four overlapping fragments of 2,552, 2,553, 3,646, and 1,589 bp, respectively. We then amplified the first half (4,896 bp) of the *Celsr3* ORF by PCR with the primer pair F5 (CGGAA TTCGC CACCA TGGCG AGGCG GCCTC TATGG TG with the EcoRI site) and R2 by using the first two fragments as templates. The PCR product was digested and cloned between the EcoRI and XbaI sites of the pCAG-Myc expression vector. The second half (5,322 bp) of the *Celsr3* ORF was cloned similarly with the primer pair F6 (ACCCA GCGGG CTACT CTTCT ACAAC) and R5 (CCCAA GCTTG AGTGA CCCTC GCTTC TGGGA AC) and inserted between the XbaI and HindIII sites. The final *Celsr3* clone was confirmed by sequencing with 16 primers covering the entire length. The cloned sequence contains a total of 36 exons, including a novel 15-nucleotide (nt) alternative exon (exon 17).

The human full-length NRSF was cloned from the HEC-1-B total RNA preparation by RT-PCR into pTNT vector (Promega) between the EcoRI and XbaI sites. The primer set was GGAAT TCAAC ATGGC CACCC AGGTA ATG and GCTCT AGATT ACTCC TGCCC TTGAG CT. The region encoding the ZF1-8 domain of NRSF was then subcloned with a Myc tag coding sequence added to the 3' end. The primers were CGGAA TTCAC CATGG GTGCT CCAGA TATT ACA and GCTCT AGATT ACAGA TCCTC TTCTG AGATG AGTTT TTGTT CGGTA ATATT ATCAC GCAA. The human full-length CTCF was cloned previously (30).

The knockdown plasmids for NRSF and *Celsr3* were constructed by ligating the annealed primer pairs into pLKO.1 (Sigma) between the EcoRI and AgeI sites. For plasmids used to generate the gel-shift probes, the human CELSR3 promoter region containing putative CTCF or NRSF motifs was amplified by PCR from the human genomic DNA and cloned into the pGEM-T vectors (Promega) (CELSR3-CTCF, ACCCA AGCTT ACCAC AGCAT CCCCG ACG and GGGGT ACCCA CCACT GCACT CCGAA AGA; CELSR3-NRSF, TCGCC GAGGT TACTT TCCTG and TTTTT GATTG GGCAC CACGG). For *in situ* hybridization, the sequences of probes for *Er81*, *Lhx6*, and *Lmo3* were amplified from the mouse brain cDNA using specific primer pairs (Allen Brain Atlas) and then cloned into pGEM-T vectors. All constructs were confirmed by sequencing.

Cell culture. HEC-1-B, HepG2, IMR-32, and SK-N-SH cells were cultured in minimal essential medium (MEM) (Gibco), supplemented with 10% fetal bovine serum (FBS) (Gibco), 1% penicillin-streptomycin (Gibco), 2 mM Glutamax (Gibco), and 1 mM sodium pyruvate (Sigma). HEK 293T cells were cultured in Dulbecco's modified Eagle medium (DMEM) (HyClone), supplemented with 10% FBS and 1% penicillin-streptomycin. Cells were maintained at 37°C in a 5% CO₂ incubator.

4C-seq. Circular chromosome confirmation capture (4C) libraries for high-throughput sequencing (4C-seq) were constructed as described previously (31), with some modifications. Briefly, an E18.5 fetal brain was dispersed by collagenase (Sigma) treatment in 500 µl of 10% FCS-DMEM for 45 min at 37°C with shaking at 700 rpm. Cells were then filtered through a 40-µm cell strainer (BD Biosciences) to make single-cell suspensions and cross-linked with 1% formaldehyde for 10 min at 37°C. Human SK-N-SH cells were cross-linked directly. The cross-linked DNA was digested with HindIII (NEB) overnight with shaking at 900 rpm and then ligated using T4 DNA ligase (NEB). After phenol-chloroform extraction and ethanol precipitation, the purified DNA was digested with the secondary restriction enzyme DpnII (NEB) and ligated again. Finally, 4C-seq libraries were amplified from the religated DNA using PCR with inverse primers, including Illumina adapter sequences (human CELSR3, AATGA TACGG CGACC ACCGA GATCT AACT CTTTC CCTAC ACGAC GCTCT TCCGA TCTCA GGAAC AGCAC CCTAC TATGG AAG and CAAGC AGAAG ACGGC ATACG AGATC GTGAT GTGAC TGGAG TTCAG ACGTG TGCTC TTCCG ATCGA ACCTA AGCAG AGTCC TTGTG AG; mouse *Celsr3*, AATGA TACGG CGACC ACCGA

GATCT ACACT CTTTC CCTAC ACGAC GCTCT TCCGA TCTCT GGTGA AGGTG CTTGG TGTCC and CAAGC AGAAG ACGGC ATACG AGATC GTGAT GTGAC TGGAG TTCAG ACCTA AGCAG AGTCC TTGTG AG; mouse *Celsr3*, AATGA TACGG CGACC ACCGA

GATCT ACACT CTTTC CCTAC ACGAC GCTCT TCCGA TCTCT GGTGA AGGTG CTTGG TGTCC and CAAGC AGAAG ACGGC ATACG AGATC GTGAT GTGAC TGGAG TTCAG ACCTA AGCAG AGTCC TTGTG AG; mouse *Celsr3*, AATGA TACGG CGACC ACCGA

GATCT ACACT CTTTC CCTAC ACGAC GCTCT TCCGA TCTCT GGTGA AGGTG CTTGG TGTCC and CAAGC AGAAG ACGGC ATACG AGATC GTGAT GTGAC TGGAG TTCAG ACCTA AGCAG AGTCC TTGTG AG; mouse *Celsr3*, AATGA TACGG CGACC ACCGA

GATCT ACACT CTTTC CCTAC ACGAC GCTCT TCCGA TCTCT GGTGA AGGTG CTTGG TGTCC and CAAGC AGAAG ACGGC ATACG AGATC GTGAT GTGAC TGGAG TTCAG ACCTA AGCAG AGTCC TTGTG AG; mouse *Celsr3*, AATGA TACGG CGACC ACCGA

GATCT ACACT CTTTC CCTAC ACGAC GCTCT TCCGA TCTCT GGTGA AGGTG CTTGG TGTCC and CAAGC AGAAG ACGGC ATACG AGATC GTGAT GTGAC TGGAG TTCAG ACCTA AGCAG AGTCC TTGTG AG; mouse *Celsr3*, AATGA TACGG CGACC ACCGA

TAATA GGAGG TTAGA AGTAG TAGTG CT; NRSF, GGATA ATGAG CGAGT CTACA AGTG and TATGG GCGTT CTCCT GTATG; GAPDH, GGAGT CCACT GGCCT CTTCA C and GCAGG AGGCA TTGCT GATGA T; mouse *Celsr3*, GCAGT CCTCA AGCAC TCCCT C and CCTGG TGGCT CCTCA TTG; mouse NRSF, CGTAT AAATG TGAAC TTTGT CCT and CCCGT TGTGA ACCTG TCTT; mouse β -actin, TTGTT ACCAA CTGGG ACGAC and CTGGG GTGTT GAAGG TCTC). Statistical analysis was performed using Student's *t* test.

Cell differentiation. The neuroblastoma IMR-32 cells were maintained at 37°C in a saturated humidity atmosphere containing 5% CO₂. After 24 h of plating, all-*trans* retinoic acid (RA) was added to a final concentration of 10 μ M to induce differentiation. Dimethyl sulfoxide (DMSO) (0.1%) was added for the vehicle control. The cells were maintained for 5 additional days, with the RA- or DMSO-containing medium being changed every 2 days.

Animals. The *Celsr3* deletion mice were previously described (11). Genotyping was performed by PCR with the primers CCCCC TGAAAC CTGAA ACATA AAATG, ACTTC AGCAC TGCAC CCGAC TTAC and GCCCT GCGAG AACTA CATGA AATG. All animal experiments were approved by the Institutional Animal Care and Use Committee (IACUC) of Shanghai Jiao Tong University.

Histology and immunohistochemistry. The day on which the vaginal plug was found was defined as E0.5. The ages of embryos were judged by the plugging date in combination with age-specific developmental features. Nissl staining was performed as described previously (11).

Dams at the appropriate pregnancy date were anesthetized with sodium pentobarbital (20 mg/ml) at a dose of 100 mg/kg. Embryos were obtained by Caesarean section of the dams. The E13.5 embryonic heads were decollated and immediately immersion fixed in cold 0.1 M phosphate-buffered saline (PBS; pH 7.4) with 4% paraformaldehyde (PFA) for 2 to 6 h. The brains of embryos older than E13.5 were removed and fixed. Adult mice were anesthetized and perfused with PBS, followed by 4% PFA in PBS. Their brains were then removed and postfixed for 4 to 6 h. After washed in PBS, the fixed brains were cryoprotected with increasing grades of sucrose (15% to 30%) in 0.1 M PBS, embedded in optimum cutting temperature compound (OCT) (Sakura), and sectioned at 14 to 20 μ m with a microtome (Leica).

For immunohistochemistry, sections were washed three times in PBS, blocked in 3% bovine serum albumin (BSA)-0.1% Triton X-100 for 1 h at room temperature (RT), and then incubated with primary antibodies at 4°C overnight. The primary antibodies used were rabbit anti-green fluorescent protein (anti-GFP) (1:2,000; Abcam), rabbit anti-GFP (1:1,000; Invitrogen), rabbit anti-tyrosine hydroxylase (anti-TH) (1:500; Millipore), rabbit anti-CR (1:2,000; Swant), rabbit anti-CB (1:3,000; Swant), rabbit anti-activated caspase 3 (1:500; Cell Signaling Technology), mouse anti-Islet1 (1:100; Developmental Studies Hybridoma Bank [DSHB]), goat anti-choline acetyltransferase (anti-ChAT) (1:100; Millipore), rabbit anti-VGLUT2 (1:1,000; Synaptic Systems), rabbit anti-Olig2 (1:500; Millipore), rabbit anti-NG2 (1:200; Millipore), mouse anti-Nkx2-1 (1:100; Labvision), mouse anti-glial fibrillary acidic protein (anti-GFAP) (1:500; Millipore), and rabbit anti-SERT (1:1,000; Immunostar).

For GFAP staining, the fixation time was shortened to 20 min. For staining with Islet1, Nkx2-1, and SERT antibodies, sections were treated by antigen retrieval in 10 mM sodium citrate (pH 6.0) before blocking. After incubation with primary antibodies, sections were washed in PBS and then incubated with Cy3- or Alexa Fluor 488-conjugated secondary antibodies (Jackson ImmunoResearch) for 1 h at RT. The sections were washed again with PBS and mounted with Vectashield DAPI-containing mounting medium (Vector Laboratories).

Acetylcholinesterase (AChE) histochemistry. For AChE histochemistry, we used the protocol described in reference 35, with minor modifications. Briefly, E18.5 brains were removed and fixed in 4% PFA in PBS for 2 h. The brains were cryoprotected with 15% and 30% sucrose, embedded in OCT, and sectioned. All the following steps were performed on a laboratory rotator at 80 rpm. After being rinsed twice in 0.1 M acetate

buffer (pH 6.0), slides were incubated in the reaction solution for 16 h in the dark. The reaction solution contained 0.12% acetylthiocholine iodide, 0.065 M sodium acetate, 4 mM sodium citrate, 3 mM cupric sulfate, and 0.1 mM potassium ferricyanide. Slides were then rinsed five times (1 min each) in the acetate buffer, incubated with 1% ammonium sulfide solution for 5 min and washed five times (1 min each) with 0.1 M sodium nitrate. Finally, slides were immersed in 0.1% silver nitrate for 5 min, followed by five changes of 0.1 M sodium nitrate and dehydrated, and coverslipped before imaging.

Cell birth dating. Pregnant dams at E10.5, E11.5, E12.5, and E13.5 received bromodeoxyuridine (BrdU) (Sigma) at 50 mg/kg with intraperitoneal injections. Embryos were harvested at E18.5. For BrdU (1:1,000; DSHB) labeling, slides were treated with HCl (2 N) for 10 min. BrdU⁺ and total cells within the GP region were quantified. The counted areas contained at least 150 cells.

Western blotting. For the analyses of Celsr3 and NRSF protein expression, P21 *Celsr3*^{+/−} brains and spleens (as a nonneural control) were removed. Brains were freshly cut at 200 μ m with a vibratome. GP, striatum, and cortex regions were then separated under a dissecting microscope. For the comparison of TH or Tau expression levels between control and *Celsr3*^{−/−} mice, the telencephalon and diencephalon were removed from E18.5 brains. These tissues were immediately homogenized in radioimmunoprecipitation assay (RIPA) buffer (Sigma) and centrifuged at 12,000 \times g for 20 min at 4°C to remove the pellets. Western blot experiments were performed according to the standard protocol, with β -actin as a loading control. The antibodies used were rabbit anti-GFP (1:1,000; Invitrogen), rabbit anti-NRSF (1:1,000; Millipore), rabbit anti-TH (1:1,000; Millipore), rabbit anti-Tau (1:1,000; Abcam), and mouse anti- β -actin (1:10,000; Abcam).

In situ hybridization. *In situ* hybridization was performed as described previously (11). Digoxigenin (DIG)-labeled cRNA probes were synthesized by *in vitro* transcriptions with T7 or SP6 polymerase. The probe targets were as follows: *Er81* (nucleotides 1781 to 2454 of NM_007960.3), *Lhx6* (nucleotides 1723 to 2126 of NM_008500.2), and *Lmo3* (nucleotides 735 to 1509 of NM_207222.2).

DiI tracing. After dissection, brains were fixed overnight with 4% PFA solution. Single crystals of 1,1'-dioctadecyl-3,3',3'-tetramethyl indo-carbocyanine perchlorate (DiI) (Molecular Probes) were inserted into various brain regions under a dissecting microscope with fine forceps.

For dorsal thalamus implantation, E13.5 and E14.5 brains were embedded in 5% agarose (Amresco). We first sectioned the brain coronally from the caudal to the rostral levels with a vibratome to expose the dorsal thalamus. Single crystals of DiI were then inserted into the dorsal thalamus using fine forceps under a dissecting microscope. The brains with DiI implanted were kept in the 4% PFA solution at RT for 2 weeks in the dark to allow dye diffusion. Finally, the brains were sectioned coronally from the dorsal thalamus toward the telencephalon at 150 μ m with a vibratome. The sections were counterstained with 4',6-diamidino-2-phenylindole (DAPI) before being imaged with a Zeiss microscope.

For striatum implantation, the agarose-embedded E18.5 brains were cut coronally from the olfactory bulb toward the striatum with a vibratome. When the striatum was exposed, single crystals of DiI were inserted. After 2 weeks of incubation with the 4% PFA solution, brains were sectioned further caudally at 150 μ m. Sections with GP were collected, counterstained with DAPI, and imaged.

For GP implantation, rostral parts of the brains were removed to expose GP. After DiI insertion, brains were kept in 4% PFA for 6 weeks at RT. Finally, the brains were sectioned caudally at 150 μ m. Sections at the desired levels were collected and imaged.

In utero electroporation. For *in utero* electroporation, we used the protocol described in reference 36, with minor modifications. Briefly, dams at E12.5 were anesthetized with pentobarbital sodium. After the abdomen had been cleaned, laparotomy was performed and the uteri were exposed. For electroporation of two vectors, a mixture of pCAG-GFP (2 μ g/ μ l) and pLKO.1-shCels3 (2.5 μ g/ μ l) or control constructs was pre-

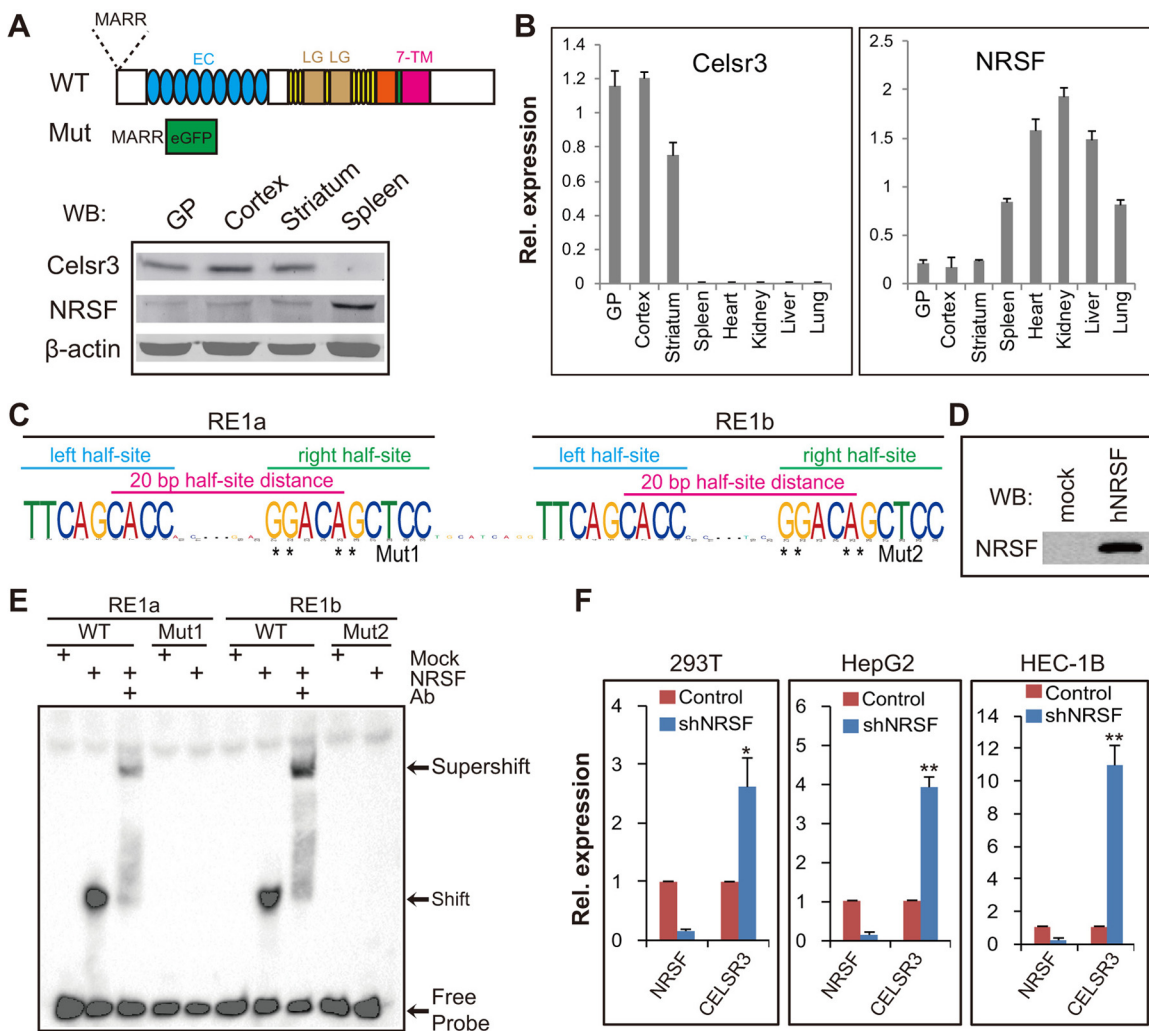


FIG 1 Inhibition of *CELSR3* expression by NRSF. (A) Schema of the wild-type (WT) and mutant (Mut) proteins and Western blot of Celsr3 and NRSF in brain tissues of the P21 *Celsr3*^{+/-} mice, with spleen as a control. EC, cadherin ectodomain; LG, Laminin-A globular domain; 7-TM, seven transmembrane segments. (B) Quantitative real-time PCR of *Celsr3* and *NRSF* in P21 mouse tissues. (C) Two noncanonical NRSF motifs located in tandem in the *CELSR3* promoter region. (D) Western blot of the *in vitro*-translated NRSF proteins. (E) Gel shift and supershift of NRSF with wild-type and mutated *NRSF* motifs. (F) Relative expression of *CELSR3* genes upon the NRSF knockdown in three different nonneuronal cell lines. Data are means \pm SD ($n = 3$). Significance was determined with Student's *t* test. *, $P < 0.05$; **, $P < 0.01$.

pared at a molar ratio of 1:1. The expression vectors were then mixed with 0.05% fast green as a tracer and injected through the uterine wall into the lateral ventricle. Five electrical pulses were applied at 32 V for a duration of 50 ms at 900-ms intervals. Six days later, the pregnant mice were sacrificed, and embryonic brains were fixed overnight. The brains were then mounted with 5% agarose and sectioned at 50 μ m with a vibratome.

Imaging and cell counting. Slides were imaged with a Zeiss Axiovert 200 microscope. The pictures in Fig. 3B, Fig. 9D, and Fig. 10D to F and H were photo merged from small pictures. Cell counting was performed on images at magnifications of $\times 200$. At least three sections of the rostral, middle, and caudal GP levels were counted. Data were expressed as means \pm standard deviations (SD). The significance of differences was assessed using the two-tailed Student *t* test.

Nucleotide sequence accession number. The sequence cloned here can be accessed through GenBank accession number KJ954288.

RESULTS

Inhibition of *CELSR3* by NRSF. To understand the mechanisms of developmental regulation of the *Celsr3* gene, we first investi-

gated the expression levels of the Celsr3 proteins in several mouse brain regions by Western blotting with an anti-enhanced-GFP (anti-eGFP) antibody using an eGFP reporter mouse line (Fig. 1A) (11). The mouse line was constructed by inserting an eGFP reporter in frame with the first four amino acid residues of the *Celsr3* protein under the control of the endogenous transcription and translational signals. We found that *Celsr3* is expressed at high levels in the GP, cortex, and striatum, in contrast to no expression in the spleen and several nonneuronal tissues (Fig. 1A and B). This is consistent with previous reports that the expression of *Celsr3* is neuron specific (37). Interestingly, we found that NRSF, which is a transcription factor suppressing the expression of neuron-specific genes in nonneuronal tissues (38), is expressed at high levels in the mouse nonneuronal tissues but at low levels in the brain (Fig. 1A and B). We found two putative NRSF binding sites located in tandem in the promoter region of *CELSR3* (Fig. 1C), although most genes contain only one NRSF binding site (39). The two sites

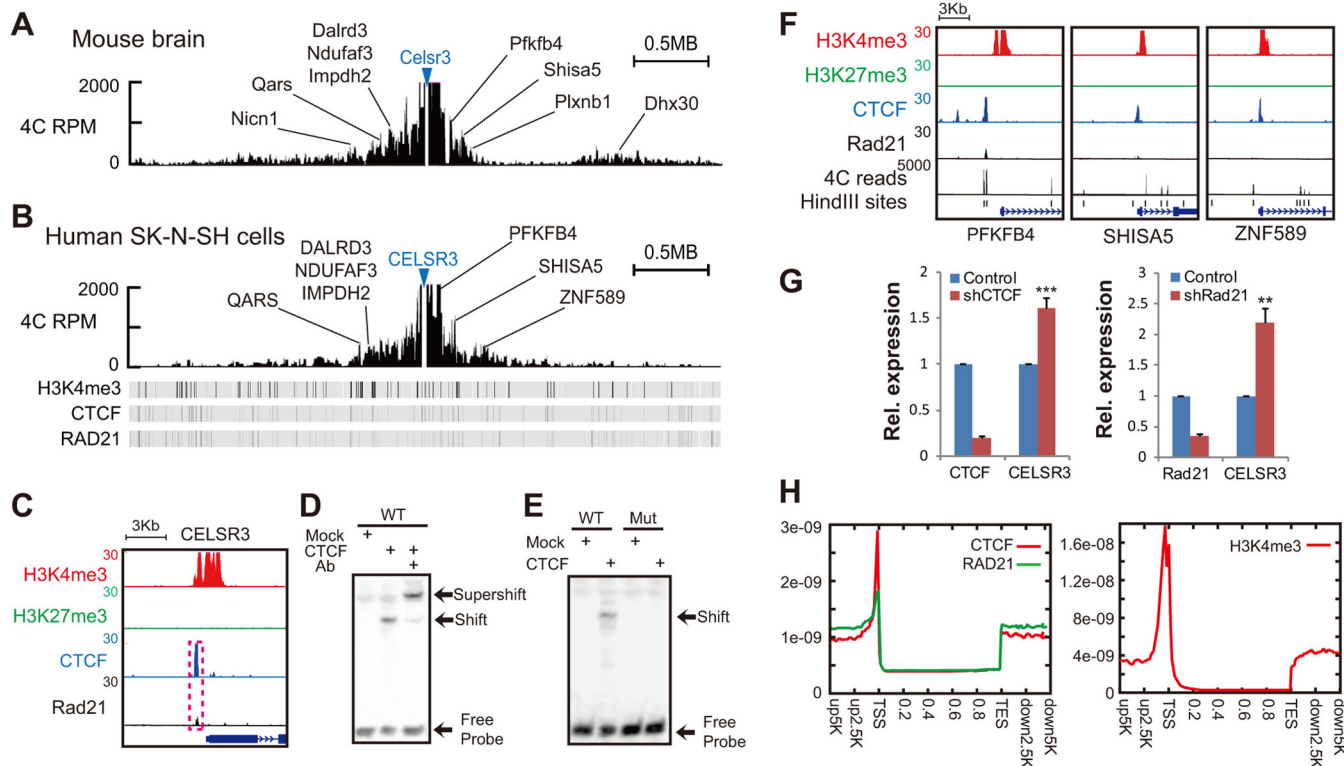


FIG 2 Spatial interactome of the *Celsr3* promoter region. (A and B) Chromosomal maps of 4C signals, in reads per million (RPM), anchored with the *Celsr3* promoter in E18.5 mouse brain tissues (A) and human SK-N-SH cells (B). (C) ChIP-seq signals of H3K4me3, H3K27me3, CTCF, and RAD21 in the *CELSR3* promoter. (D and E) Gel shift and supershift of CTCF with wild-type (WT) or mutated (Mut) probes of *CELSR3*. (F) Read density of H3K4me3, H3K27me3, CTCF, and RAD21, as well as 4C signals, in three interacting promoters. (G) Relative expression of *CELSR3* upon CTCF and RAD21 knockdown. (H) Genome-wide localization of CTCF, RAD21, and H3K4me3 immediately upstream of TSS. Data are means \pm SD ($n = 3$). Significance was determined with Student's *t* test. **, $P < 0.01$; ***, $P < 0.001$.

contain exactly the same binding motifs (Fig. 1C). Gel shift and supershift experiments with recombinant NRSF showed that it binds to both motifs (Fig. 1D and E). Knockdown of NRSF in several nonneuronal cell lines results in significant increases of *CELSR3* expression (Fig. 1F). Thus, NRSF binds directly to the *CELSR3* promoter region and inhibits its expression.

Role of CTCF and cohesin in *CELSR3* gene regulation. To further investigate the mechanisms of *Celsr3* gene regulation, we performed 4C-seq experiments by using the *Celsr3* promoter region as an anchor in the mouse brain as well as in the human neural cell line SK-N-SH. We found that the *Celsr3* promoter is looped with the promoter regions of several neighboring genes as well as several nonpromoter regions in the mouse brain (Fig. 2A). Similarly, the human *CELSR3* promoter also interacts with promoters of several neighboring genes (Fig. 2B). ChIP-seq experiments revealed that all of these looped promoters are occupied by the active histone mark H3K4me3 (Fig. 2B). In particular, the *CELSR3* promoter is marked by H3K4me3 as well as the chromosomal architectural proteins CTCF and cohesin subunit RAD21 (Fig. 2C). Manual inspections identified a putative CTCF-binding motif in the *CELSR3* promoter region. Gel shift experiments showed that CTCF and the motif form a retarded band which is supershifted with a CTCF-specific antibody and is abolished by mutation of the core sequences (Fig. 2D and E). We noted that the vast majority of the looped promoters are enriched with CTCF and RAD21 (Fig. 2B and F). Finally, knockdown of CTCF or

RAD21 results in significant increases of *CELSR3* expression (Fig. 2G). Importantly, genome-wide analysis revealed that CTCF/cohesin complexes, as well as the H3K4me3 mark, are specifically enriched immediately upstream of transcription start sites (TSS) in SK-N-SH cells (Fig. 2H), suggesting an architectural role of CTCF/cohesin in mediating genome-wide promoter-promoter interactions. Taken together, we conclude that CTCF-mediated chromatin looping interactions between neighboring promoters are important in the regulation of *Celsr3* gene expression.

***Celsr3* expression patterns in GP.** To investigate whether *Celsr3* expression is regulated during neural differentiation, we used retinoic acid (RA) to induce differentiation of the human neuroblastoma cell line IMR-32. We found significant increases of human *CELSR3* expression upon RA-induced differentiation of IMR-32 cells (Fig. 3A), consistent with a previous report that *Celsr3* is expressed in differentiated brain nuclei (37). Interestingly, we found that *Celsr3* is especially enriched in the differentiated ventral forebrain nuclei of the GP in the developing mouse embryos (Fig. 3B). Costaining with the GP marker Nkx2-1 (21, 23) demonstrated that the vast majority of GP cells express *Celsr3* (Fig. 3C to E). Quantification revealed that $77.2\% \pm 2.8\%$ ($n = 3$ mice) of Nkx2-1 $^{+}$ (GP) cells express *Celsr3* at E15.5 (out of 506 Nkx2-1 $^{+}$ cells quantified, 391 cells are *Celsr3* $^{+}$), $85.7\% \pm 4.6\%$ ($n = 8$ sections from 3 mice) at E18.5 (out of 675 Nkx2-1 $^{+}$ cells quantified, 578 cells are *Celsr3* $^{+}$), and $97.0\% \pm 1.0\%$ ($n = 8$ sections from 3 mice) in the adult (out of 327 Nkx2-1 $^{+}$ cells quantified).

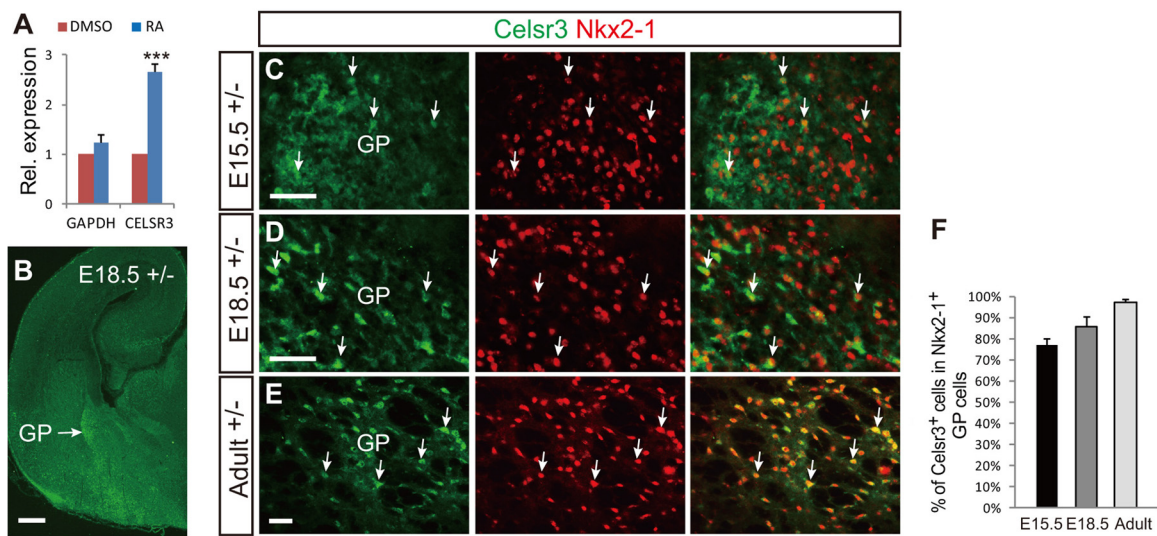


FIG 3 Prominent expression of *Celsr3* in GP. (A) Expression level of *Celsr3* in RA-treated IMR-32 cells. (B) *Celsr3* expression pattern in the mouse forebrain. (C to E) Expression of *Celsr3* (green) and *Nkx2-1* (red) in GP. Examples of coexpressed cells are indicated by arrows. (F) Quantification of the expression of *Celsr3* in *Nkx2-1*⁺ GP cells. Data are means \pm SD ($n = 3$ mice). Significance was determined with Student's *t* test. ***, $P < 0.001$. Scale bars, 300 μm (B) and 50 μm (C to E).

fied, 318 cells are *Celsr3*⁺) (Fig. 3F). This prominent expression of *Celsr3* in the GP suggests that *Celsr3* may play an important role in GP development and function.

Abnormal GP in *Celsr3* mutant mice. To investigate whether there are developmental defects of the GP in *Celsr3*-targeted mice, we performed DAPI and Nissl staining and found that an aberrant region where cells are sparse appears at E14.5 in the developing ventral GP of the *Celsr3* mutant mice (Fig. 4A). In addition, this defect is progressively more pronounced from E14.5 to E18.5 (Fig. 4A). Finally, we found many more GFAP⁺ astrocytes in the mutant GP than in the control, suggesting reactive gliosis resulting from potential increases of apoptosis (Fig. 4B). Indeed, activated caspase 3 immunostaining showed an increase of apoptosis in the mutant GP (Fig. 4C).

We analyzed the GP defect with its marker *Nkx2-1* by serial coronal sectioning from rostral to caudal levels and found that the distribution of *Nkx2-1*⁺ cells is disrupted by the same region with sparse cells (Fig. 4A and D). In particular, this region appears at the middle and caudal levels (Fig. 4D). Quantification revealed that the densities of *Nkx2-1*⁺ cells increase in the mutant dorsal GP but decrease in the mutant ventral GP (Fig. 4E). In addition, the difference in cell densities is progressively more pronounced from the middle to caudal levels (Fig. 4D and E).

Aberrant CB⁺ cells in the mutant GP. To investigate the etiology of the abnormal GP morphology, we performed *in situ* hybridization with a set of GP-specific transcription factor genes, such as *Er81*, *Lhx6*, and *Lmo3* (23). We found that mutant GP cells maintain the same levels of their expression, suggesting no fate determination defects in GP (Fig. 5A). In addition, we performed immunostaining with Olig2 and NG2, which are oligodendrocyte markers in GP (23), and found no change of oligodendrocytes in the mutant GP (Fig. 5B and C). Third, we performed birth-dating experiments with BrdU injection at E10.5, E11.5, E12.5, and E13.5, which are the main stages of GP neurogenesis (21), and found no difference in birth timing of GP cells (Fig. 5D). Finally, we performed CB staining and found aberrant CB⁺ cells in the

mutant ventral GP (Fig. 5E). These CB⁺ cells in the mutant ventral GP have relatively big soma with leading processes pointing in different directions (Fig. 5E). Surprisingly, these CB⁺ cells do not express the GP marker *Nkx2-1* (Fig. 5F). This suggests that the CB⁺ cells in the mutant GP are of ectopic origin.

CB⁺ cells are cholinergic neurons. GP contains cholinergic neurons that represent an extension from the basal magnocellular complex (Ch4) (21). This Ch4 complex comprises cholinergic neurons scattered throughout the ventral pallidum, ansa lenticularis, substantia innominata, magnocellular preoptic nucleus (MCPO), and NB (40, 41). To determine the origin of the CB⁺ cells in the mutant ventral GP, we performed costaining with CB and ChAT, a marker of cholinergic neurons, and found that most of the CB⁺ cells in the mutant ventral GP are ChAT⁺ (Fig. 6A). Quantification showed that the vast majority of CB⁺ cells (88.9% \pm 7.6%; $n = 3$ mice) coexpress ChAT (out of 118 CB⁺ cells quantified, 103 cells are ChAT⁺) (Fig. 6B). Consistently, AChE histochemistry showed that the mutant ventral GP has more AChE signals than controls at the middle to caudal levels (Fig. 6C). Quantification revealed that cholinergic cells in the mutant GP are significantly increased, especially at the middle to caudal levels (Fig. 6D). Together, these data demonstrated that CB⁺ cells in the mutant ventral GP are cholinergic neurons.

Aberrant CB⁺ ChAT⁺ cells are of ectopic origin. The expression of the LIM-homeobox transcription factor Islet1 is specifically excluded from GP (42). However, there are aberrant Islet1 expression patterns in the mutant ventral GP (Fig. 7A). Costaining of CB and Islet1 revealed that the vast majority of CB⁺ cells (91.6% \pm 3.7%; $n = 3$ mice) in the mutant ventral GP also express Islet1 (out of 69 CB⁺ cells quantified, 63 cells are Islet1⁺) (Fig. 7B and C). We costained ChAT and Islet1 and found that they are coexpressed in the mutant ventral GP (Fig. 7D). Quantification revealed that 81.2% \pm 4.1% ($n = 3$ mice) of cholinergic neurons in the mutant ventral GP coexpress Islet1 (out of 137 ChAT⁺ cells quantified, 111 cells are Islet1⁺) (Fig. 7E). The property of coexpression of ChAT and Islet1 of these aberrant cells in the mutant is

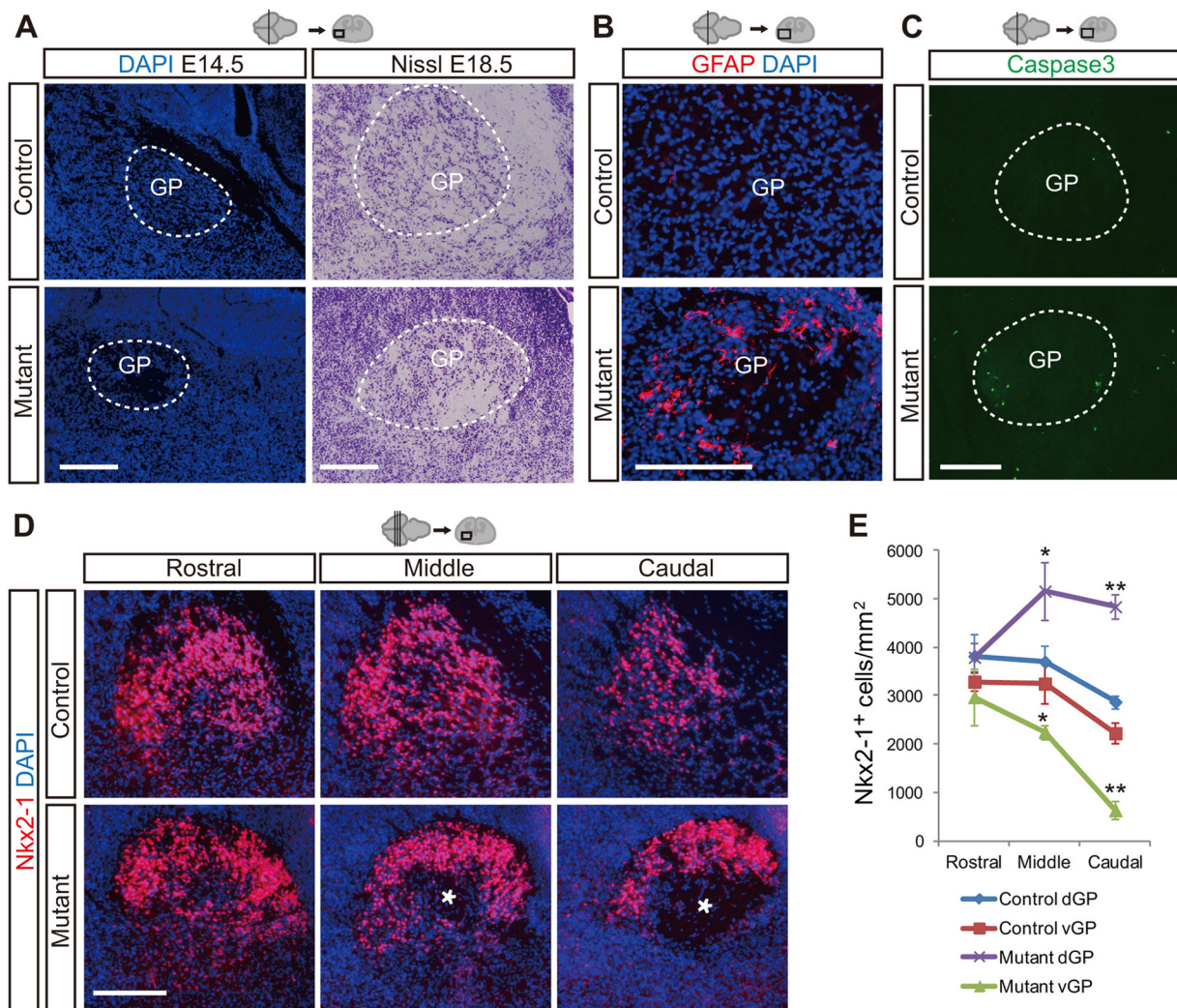


FIG 4 Abnormal GP morphology in *Celsr3* mutant mice. (A) DAPI and Nissl staining of the E14.5 and E18.5 GP, respectively. The GP region is indicated. (B) GFAP staining of the E18.5 GP. (C) Activated caspase 3 staining of the E18.5 GP. (D) Nkx2-1 and DAPI staining of the E18.5 GP at different rostrocaudal levels. The asterisk indicates the abnormal region with sparse cells in the mutant ventral GP. (E) Quantification of the Nkx2-1⁺ cell densities in the dorsal and ventral GP at different rostrocaudal levels. dGP, dorsal GP; vGP, ventral GP. Data are means \pm SD ($n = 3$ mice). Significance was determined with Student's *t* test. *, $P < 0.05$; **, $P < 0.01$. Scale bars, 200 μ m.

similar to that of ChAT⁺ Islet1⁺ NB cells in the control (Fig. 7D and E). Collectively, the data lead us to conclude that these aberrant CB⁺ ChAT⁺ Islet1⁺ cells are of ectopic origin.

Ectopic CB⁺ ChAT⁺ Islet1⁺ neurons are from NB. We found that the vast majority of cholinergic neurons in NB and MCPO express *Celsr3* (Fig. 8A and B). However, CB is expressed in cholinergic neurons from NB (43) but not MCPO, consistent with the fact that there is no difference between the MCPO regions of mutant and control mice (Fig. 8C). The strong expression of CB by the cholinergic neurons in the mutant ventral GP (Fig. 6A) suggests that these neurons may be ectopic from NB. Indeed, the region ventral to GP contains numerous cholinergic NB neurons in control mice (Fig. 8D). In mutant mice, however, the cholinergic neurons of NB appear to be located within the ventral GP, and there are no cholinergic neurons ventral to GP (Fig. 8D). As Islet1 is expressed in about 80% of cholinergic neurons in NB in the ventral telencephalon (41) (Fig. 7D and E), and taking this in conjunction with the fact that NB is absent in the corresponding

region of the mutant mice (Fig. 8D), we concluded that the ChAT⁺ CB⁺ Islet1⁺ neurons in the mutant ventral GP are ectopic from NB, as shown in the schema in Fig. 8E. To see whether *Celsr3* plays cell-autonomous or non-cell-autonomous roles in GP, we transiently expressed *Celsr3* in GP by *in utero* electroporation and found that the ventral GP still has similar defects (Fig. 8F), suggesting a non-cell-autonomous role of *Celsr3* that is consistent with its known cell adhesion activities (2).

Missing guidepost cells in the caudal GP. Expression of *Celsr3* in the basal forebrain is required for the thalamocortical axon (TCA) pathfinding (8, 10). However, the underlying mechanisms are unknown. It has been proposed that cells associated with developing internal capsule (IC cells) act as transient guideposts for TCA pathfinding (25–28, 44). We first confirmed the role of *Celsr3* in the development of thalamocortical connections by transiently knocking down *Celsr3* in the ventral forebrain through *in utero* electroporation using CR as a marker for TCA (Fig. 9A and B) (8, 10, 42). Second, we found that Nkx2-1⁺ cells in the mutant GP

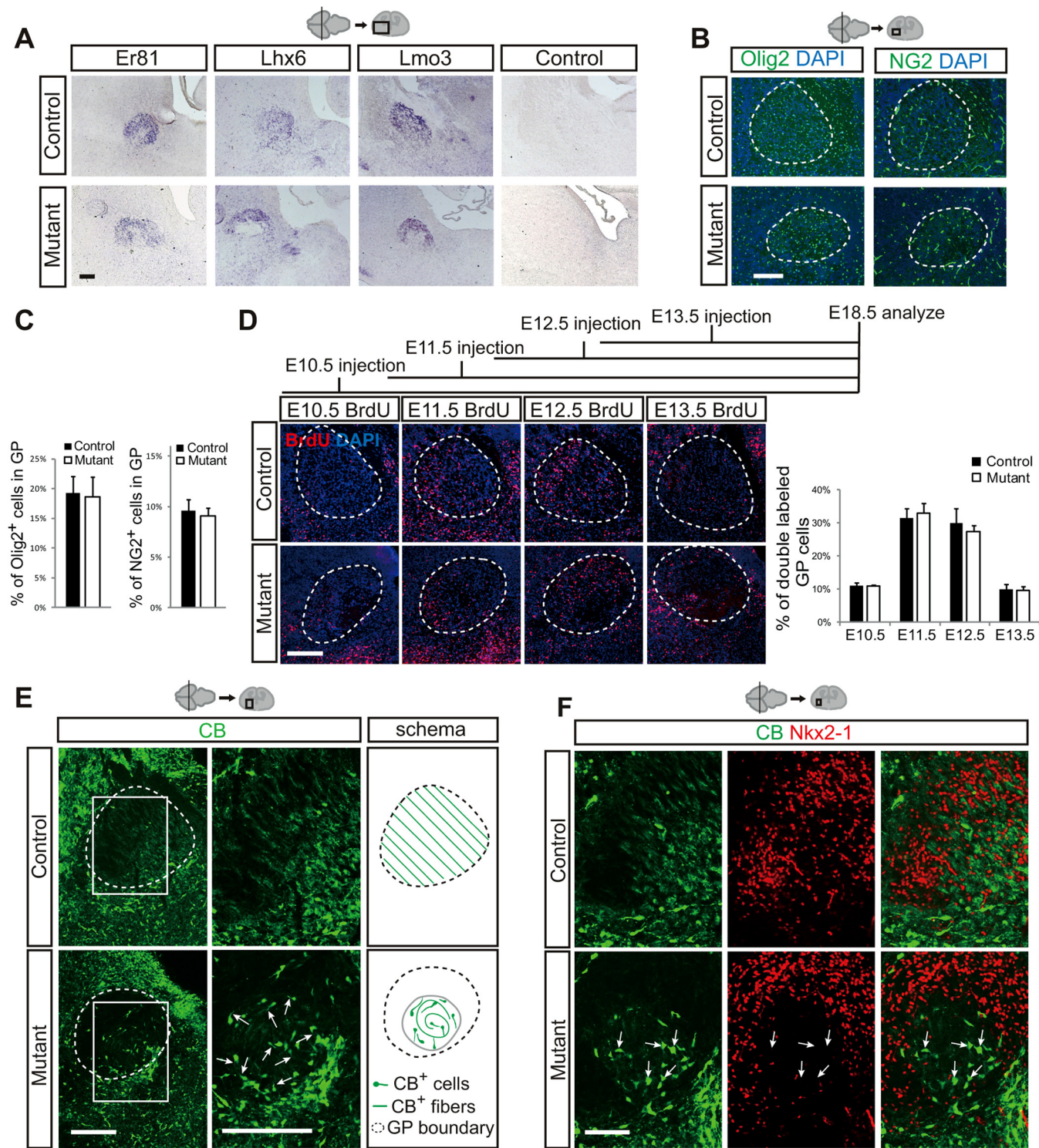


FIG 5 Aberrant CB⁺ cells in the mutant ventral GP. (A) *In situ* hybridization of *Er81*, *Lhx6*, and *Lmo3* with a sense probe as the control. (B and C) Olig2 and NG2 staining (B) and quantification (C) of the oligodendrocytes in the GP. (D) Birth dating of the GP cells with BrdU injected at E10.5, E11.5, E12.5, and E13.5. (E) CB staining and the schema of the E18.5 control and mutant GP. Abnormal CB⁺ cells are indicated by arrows. (F) CB and Nkx2-1 staining of GP. Note that CB and Nkx2-1 are not colocalized (arrows). Data are means \pm SD ($n = 3$ mice). Scale bars, 200 μ m (A to E) and 100 μ m (F).

cannot extend caudally at E13.5 and E14.5 (Fig. 9C), stages coinciding with those when TCA makes a sharp turn to the basal forebrain from the thalamus (42). The Nkx2-1⁺ cells in the caudal extension of GP send axons to the dorsal thalamus to guide the

TCA development and are the so-called IC cells (26–29, 45, 46). Finally, by inserting DiI in the E13.5 and E14.5 dorsal thalamus, we found no retrogradely labeled cells in the mutant basal forebrain, suggesting the absence of guidepost IC cells (Fig. 9D). To-

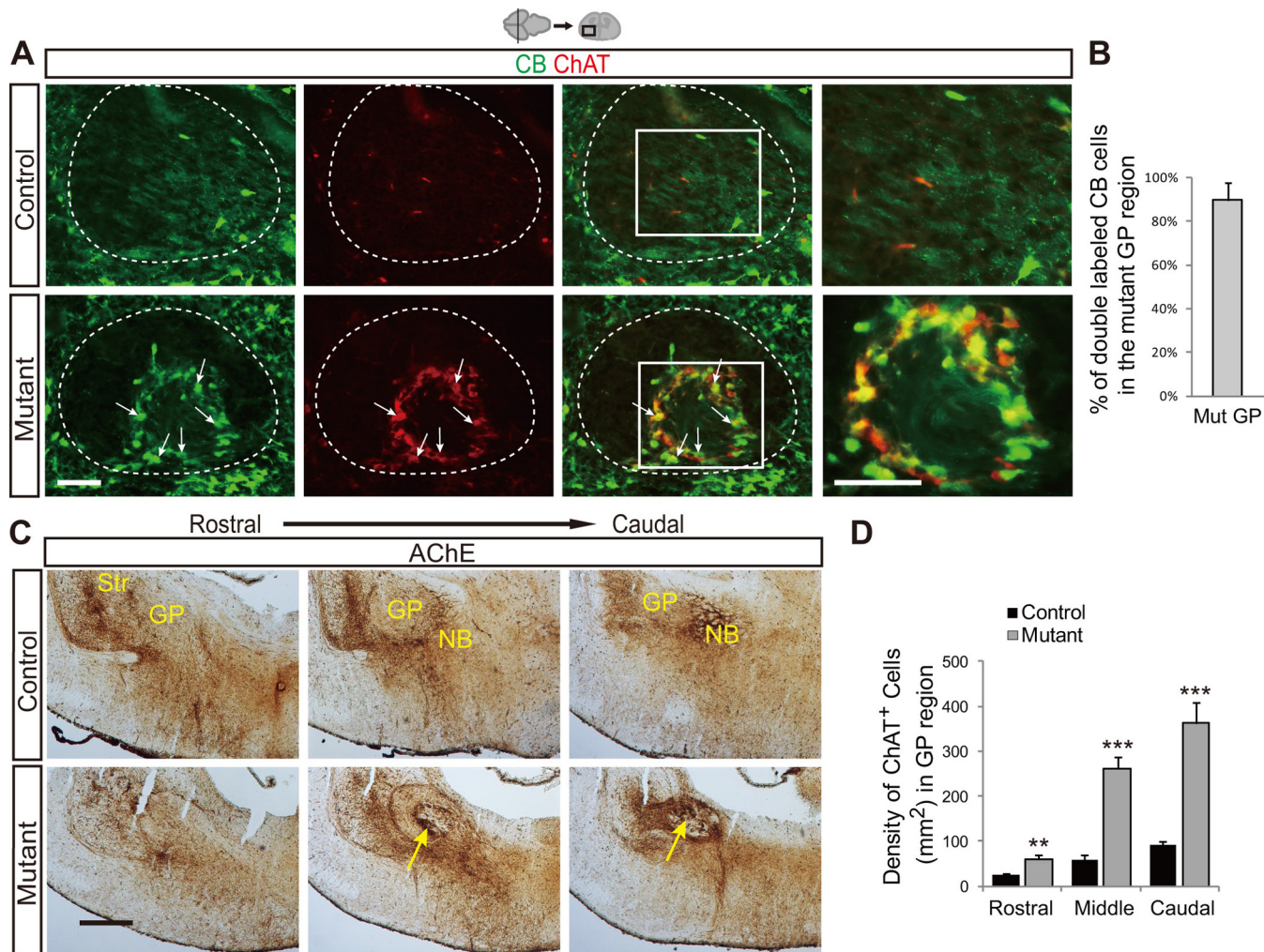


FIG 6 CB⁺ cells in the mutant GP are cholinergic neurons. (A) CB and ChAT staining of the E18.5 GP. Costained CB⁺ ChAT⁺ neurons are indicated by arrows. (B) Quantification of ChAT⁺ CB⁺ neurons in the mutant GP. (C) AChE labeling of the ventral telencephalon. Note the aberrant AChE signals in the mutant middle and caudal GP (arrows). (D) Quantification of the density of ChAT⁺ neurons in the rostral, middle, and caudal GP. NB, nucleus basalis. Data are means \pm SD ($n = 3$ mice). Significance was determined with Student's *t* test. **, $P < 0.01$; ***, $P < 0.001$. Scale bars, 100 μ m (A) and 400 μ m (C).

gether, these data lead us to propose that the absence of caudal GP IC cells underlies the TCA pathfinding defects in the *Celsr3* mutant mice.

Absence of GP axonal connections. In addition to the absence of IC cells causing TCA pathfinding defects, we found novel GP axonal connection defects with several brain nuclei. Specifically, staining with antibodies against CR, VGLUT2, TH, and SERT revealed no signals in the E18.5 mutant GP, suggesting dramatic defects of multitude afferent axonal projections to the GP from other brain nuclei such as the forebrain STN, midbrain SNC, and hindbrain dorsal raphe (Fig. 10A). To see whether it was caused by axonal pathfinding defects or axon degeneration after the connections had been established, we analyzed CR⁺, VGLUT2⁺, TH⁺, and SERT⁺ axonal fibers in the E15.5 and E13.5 GP. We found that the mutant GP is free of these axons at both stages (Fig. 10B and C), suggesting that *Celsr3* affects the early axonal pathfinding.

To confirm the axonal connectivity defects, we performed Dil tracing experiments by inserting Dil in GP or striatum. We found that Dil inserted in GP resulted in no signals in EP, STN, and SN in mutants compared with strong signals in controls (Fig. 10D). In

addition, Dil inserted in striatum resulted in no signals in the mutant GP (Fig. 10E). Taken together, these data indicate that there is no axonal connectivity between GP and other brain nuclei.

To investigate the underlying mechanism of GP axonal pathfinding defects, we stained sagittal sections with the TH antibody and found that TH axons from SNC cannot pass through the telencephalon-diencephalon boundary (TDB) and instead turn ventrally toward the hypothalamus (Fig. 10F). Western blot confirmed the absence of TH proteins in the telencephalon (Fig. 10G). In fact, CR⁺, VGLUT2⁺, and SERT⁺ axons all have similar defects (Fig. 10H). Thus, we propose that these axons projecting to GP from discrete brain nuclei are stalled at the TDB (Fig. 10I).

DISCUSSION

GP plays a central role in the neural circuits of BG, and its dysfunctions cause a repertoire of devastating heterogeneous neurological disorders (19, 47, 48). Here, we report that the protocadherin gene *Celsr3*, a member of core mammalian PCP genes, is regulated by transcription factors CTCF and NRSF and is required for GP development. We found that the ventral GP is occupied by

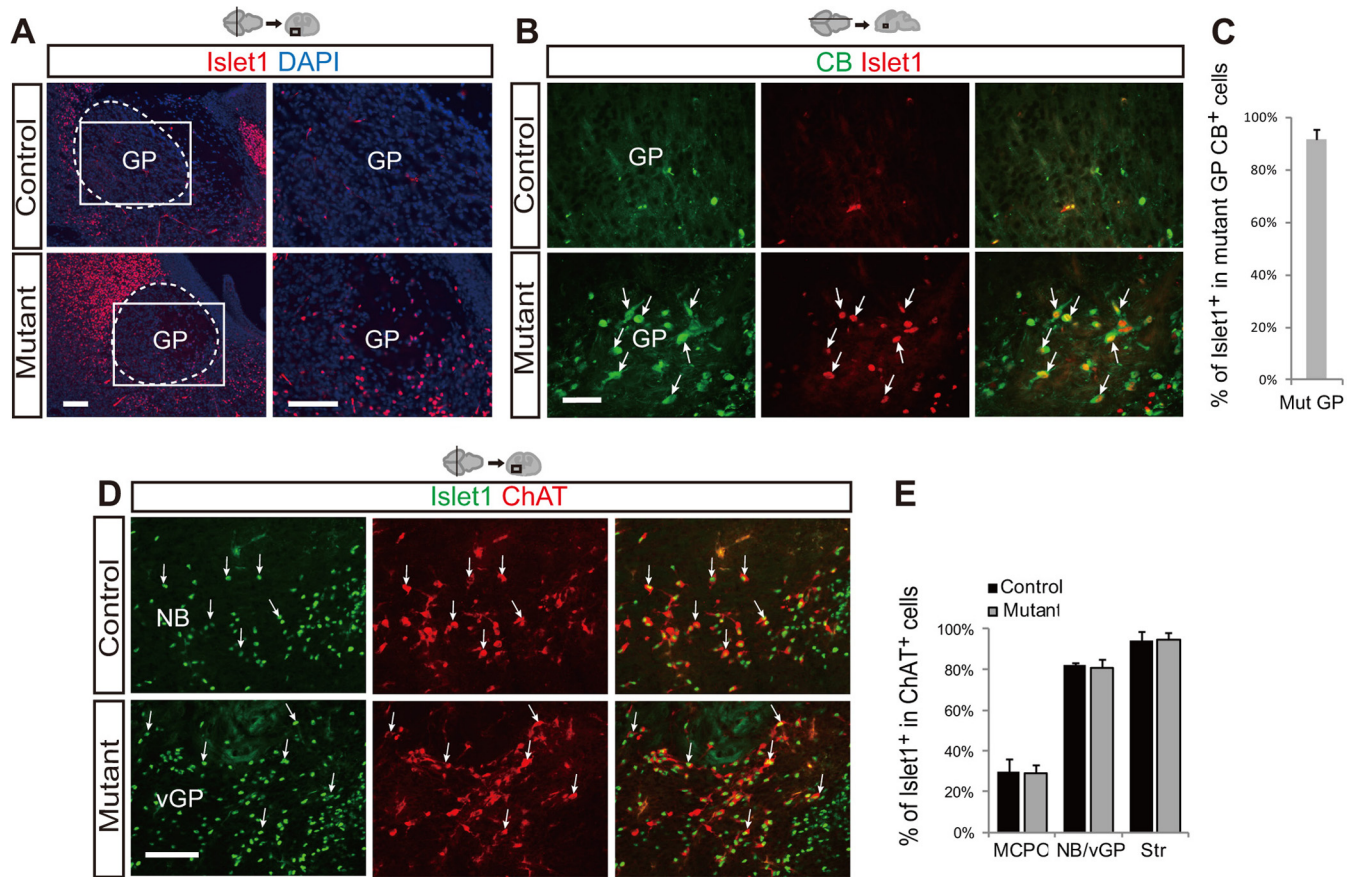


FIG 7 CB⁺ ChAT⁺ cells in the mutant are not endogenous GP cells. (A) Islet1 expression pattern in striatum and GP. Note the exclusion of Islet1⁺ cells in the control but not the mutant GP. (B) Costaining of CB and Islet1 (coexpressing cells are indicated by arrows). (C) Quantification of CB and Islet1 coexpression. (D) Coexpression of Islet1 and ChAT in the control NB and mutant ventral GP. (E) Quantification of the percentages of Islet⁺ cells in different cholinergic neuron groups. MCPO, magnocellular preoptic nucleus; NB, nucleus basalis. Data are means \pm SD ($n = 3$ mice). Scale bars, 100 μ m.

aberrant cholinergic cells ectopic from NB. Furthermore, we provide evidence that *Celsr3* is required for the development of axonal projections between GP and the brain nuclei of the striatum, EP, STN, SN, and raphe. Taken together, our data reveal a new role of the protocadherin gene *Celsr3* in the morphogenesis of GP and provide mechanistic insights into the axonal guidance in the brain.

The *Pcdh* genes constitute a large subfamily of the cadherin superfamily that are expressed mainly in the central nervous system in a cell- or tissue-specific or developmental-stage-specific manner (49, 50). In particular, the clustered *Pcdh* genes are organized into variable and constant regions and generate enormous neural diversity by stochastic promoter choice combined with alternative pre-mRNA splicing (51–53). Recently, the neural expression of the clustered *Pcdh* genes was found to be controlled by both CTCF and NRSF (30, 38, 54, 55). In particular, the CTCF/cohesin complex plays a pivotal role in the promoter choice of the clustered *Pcdh* genes by mediating specific DNA looping interactions between enhancers and selective variable promoters (30). However, virtually nothing is known about the developmental regulation of members of the *Celsr* subfamily of nonclustered *Pcdh* genes. Here, we found that the *Pcdh Celsr3* gene is regulated by both the insulator CTCF and the repressor NRSF. Specifically, by a combination of bioinformatics analyses and biochemical exper-

iments, in conjunction with genome-wide ChIP-seq and 4C-seq, we found that NRSF binds to two sites and CTCF binds to one site in the *Celsr3* promoter region and that the *Celsr3* promoter interacts with several neighboring promoters through long-distance DNA looping. This suggests that CTCF/cohesin-mediated chromatin looping is involved in the regulation of the *Celsr3* gene. Interestingly, recent chromatin interaction analysis with paired-end tag sequencing (ChIA-PET) experiments revealed widespread CTCF-mediated promoter-promoter or promoter-enhancer interactions (56), and Hi-C experiments revealed largely invariant topologically associating domains (TADs) in different human and mouse cell types or tissues (57). Given the enrichment of CTCF and localization of the active histone mark H3K4me3 in the promoter regions of *Celsr3* and several neighboring genes (Fig. 2C and F), these genes may be coregulated in a TAD by CTCF. Finally, our data suggested that, in nonneuronal cells, NRSF represses the expression of *Celsr3* by binding directly to its promoter (Fig. 1). However, there is no NRSF binding site in the promoter regions of the *Celsr1* and *Celsr2* genes, and knockdown of CTCF in SK-N-SH results in no alteration of *Celsr2* gene expression (data not shown), suggesting that CTCF and NRSF specifically regulate *Celsr3* but not *Celsr2*.

In the basal forebrain, CB⁺ cells are heterogeneous, and one subtype is cholinergic neurons (43). We found that CB⁺/ChAT⁺

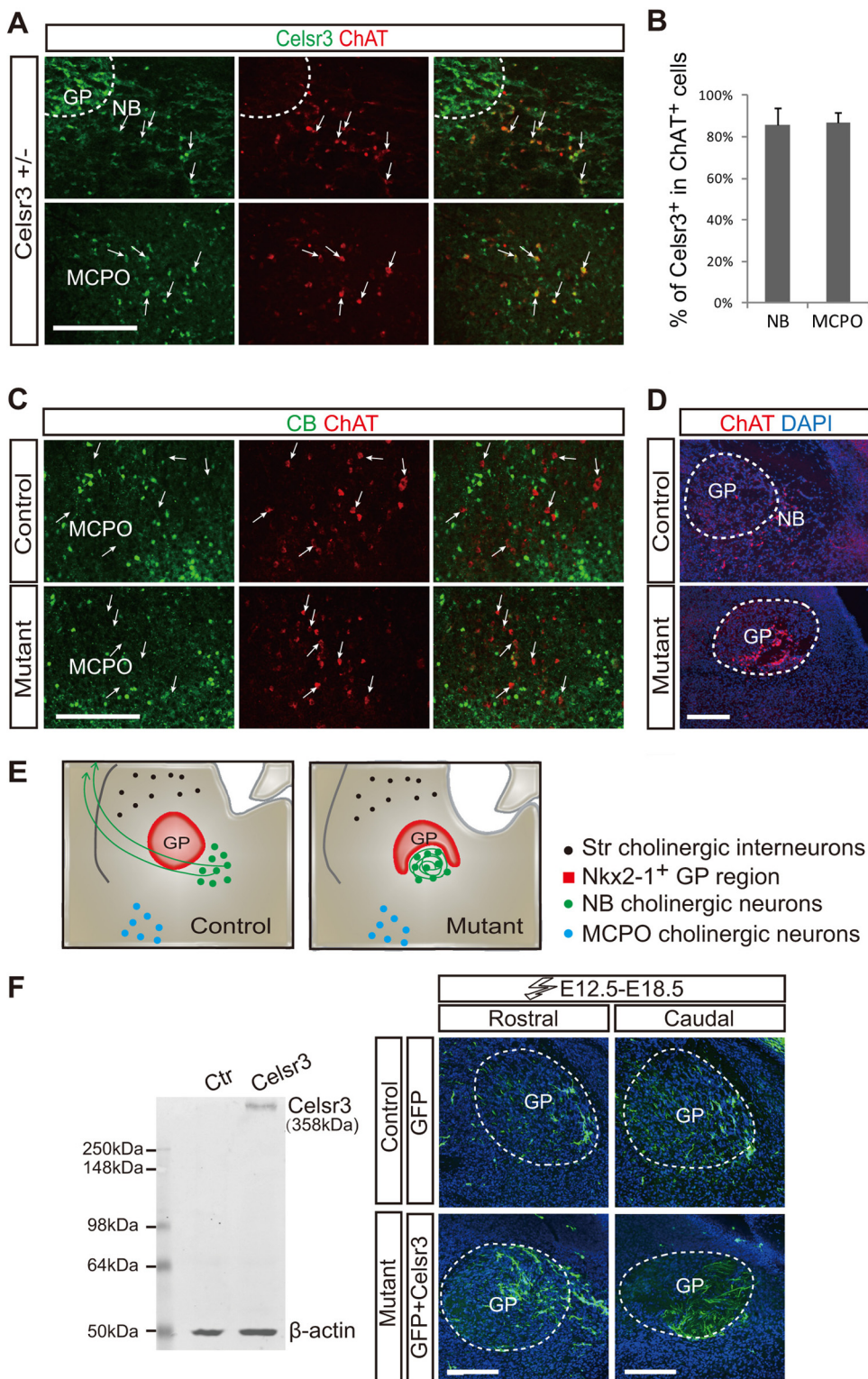


FIG 8 Aberrant CB⁺ ChAT⁺ cells are ectopic from NB. (A and B) Coexpression of Celsr3 and ChAT (A) and its quantification (B) in NB and MCPO cholinergic neurons. (C) Costaining of CB and ChAT. Note that most cholinergic neurons in MCPO are CB negative. (D) ChAT and DAPI staining showing relative positions of GP and NB. (E) Schema of the *Celsr3* mutant model. (F) Western blot confirmation of the recombinant Celsr3 expression and *in utero* electroporation of Celsr3 into the mutant GP. Data are means ± SD ($n = 3$ mice). Scale bars, 200 μ m.

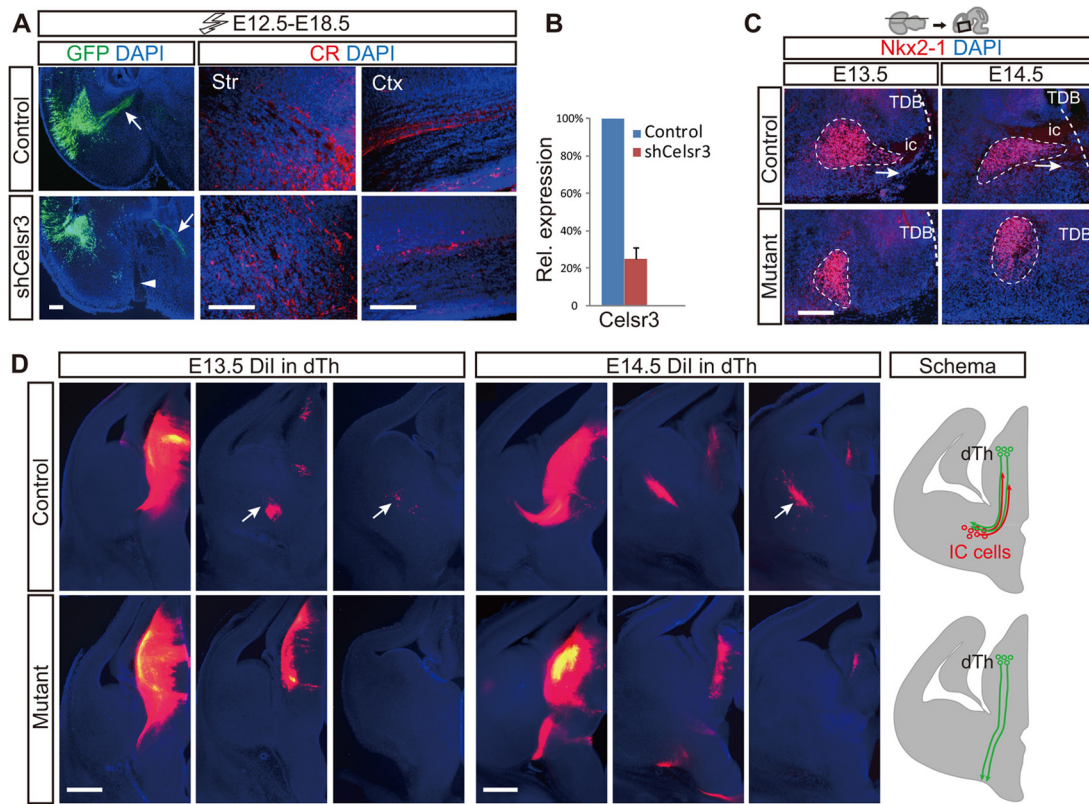


FIG 9 Absence of IC guidepost cells in the mutant ventral forebrain. (A) *Celsr3* knockdown in the basal forebrain by *in utero* electroporation. CR staining showed the decrease of CR⁺ TCA projections in the striatum and cortex. (B) Knockdown efficiency of shCelsr3. (C) Nkx2-1 and DAPI staining of the E13.5 and E14.5 basal forebrain. (D) Retrograde tracing of IC cells (arrows) by inserting Dil in the E13.5 and E14.5 dorsal thalamus and sectioning rostrally, with a schema. TDB, telencephalon-diencephalon boundary; ic, internal capsule. Scale bars, 200 μ m (A and C) and 400 μ m (D). Data are means \pm SD ($n = 3$).

cells are mislocalized in the ventral GP of the *Celsr3* mutant forebrain. There are four groups of cholinergic neurons in the ventral telencephalon that originate from both subpallium and pallium (22, 58, 59). Ch1 neurons in the medial septum and Ch2 neurons in the vertical limb of the diagonal band project to the hippocampus. Ch3 neurons in the horizontal limb of the diagonal band project to the olfactory bulb. Ch4 neurons from the basal magnocellular complex project to the neocortex (40, 60). The basal magnocellular complex includes NB and MCPO. Abnormality of Ch4 neurons causes impairment in attention and memory, which are implicated in cognitive defects in Parkinson's and Alzheimer's diseases (61).

Without *Celsr3*, ectopic cholinergic cells are aberrantly localized in the ventral GP. These ectopic Ch4 neurons appear to be specifically from NB but not from MCPO. First, although Ch4 neurons in both NB and MCPO express *Celsr3* (Fig. 8A and B), the Ch4 neurons in MCPO are not altered by the loss of *Celsr3* (Fig. 8C). Second, in contrast to NB cells, MCPO cells do not coexpress CB and ChAT (Fig. 8C) (43). Finally, while about 80% of cholinergic neurons in NB express Islet1 (Fig. 7D and E) (41), only about 30% of ChAT⁺ cells express Islet1 in the MCPO (Fig. 7E) (41). Thus, these CB⁺ ChAT⁺ Islet1⁺ neurons in the mutant ventral GP are ectopic from NB but not MCPO.

The ventral telencephalon is central for axonal projections of TCA and corticothalamic axon (CTA) (62). For example, the GP in the mantle zone of the MGE constitutes a critical decision region for the early projection of TCA (25, 29, 62). The

Nkx2-1 gene is a specific marker for GP, and the Nkx2-1⁺ cell domain in the mantle region of the MGE is equivalent to that of the GP (22, 27, 28).

The Nkx2-1⁺ GP region transiently extends a caudal cell domain associated with the internal capsule (IC) at the early embryonic stage of E13.5 to E14.5 (Fig. 9C) (27). This Nkx2-1⁺ cell domain, referred to as VTel1 (27), is required for TCA to cross the TDB and reach the internal capsule of the ventral telencephalon (27–29, 46, 63). The TCA then traverses the internal capsule corridor in close proximity to GP en route to the cortex (42, 64). Their projections are thought to be guided by the so-called guidepost cells, aka Nkx2-1⁺ IC cells, to pass through TDB and the Islet1⁺ corridor (27–29, 42, 46). The phenotype of absence of caudal extension of Nkx2-1⁺ IC cell domain in the Pcdh *Celsr3* mutant is very similar to that of the *Pcdh10* mutant (28). Due to this defect, TCA cannot cross the crucial TDB (28; also this study). Thus, our data demonstrate a critical role of *Celsr3* in patterning axonal guidance cues and provide a mechanistic insight into the function of *Celsr3* in TCA pathfinding.

Both clustered *Pcdh* genes and nonclustered *Pcdh* genes play roles in diverse cellular functions in neurodevelopment, such as cell adhesion (65), neuronal migration (11, 13), dendrite development (9, 66, 67), spine morphogenesis (66), axon outgrowth (8, 10, 68, 69), and synaptogenesis (70). The molecular mechanisms underlying these diverse cellular processes are not known; however, they may regulate actin cytoskeletal dynamics through molecular switches of small GTPase proteins (66). In particular,

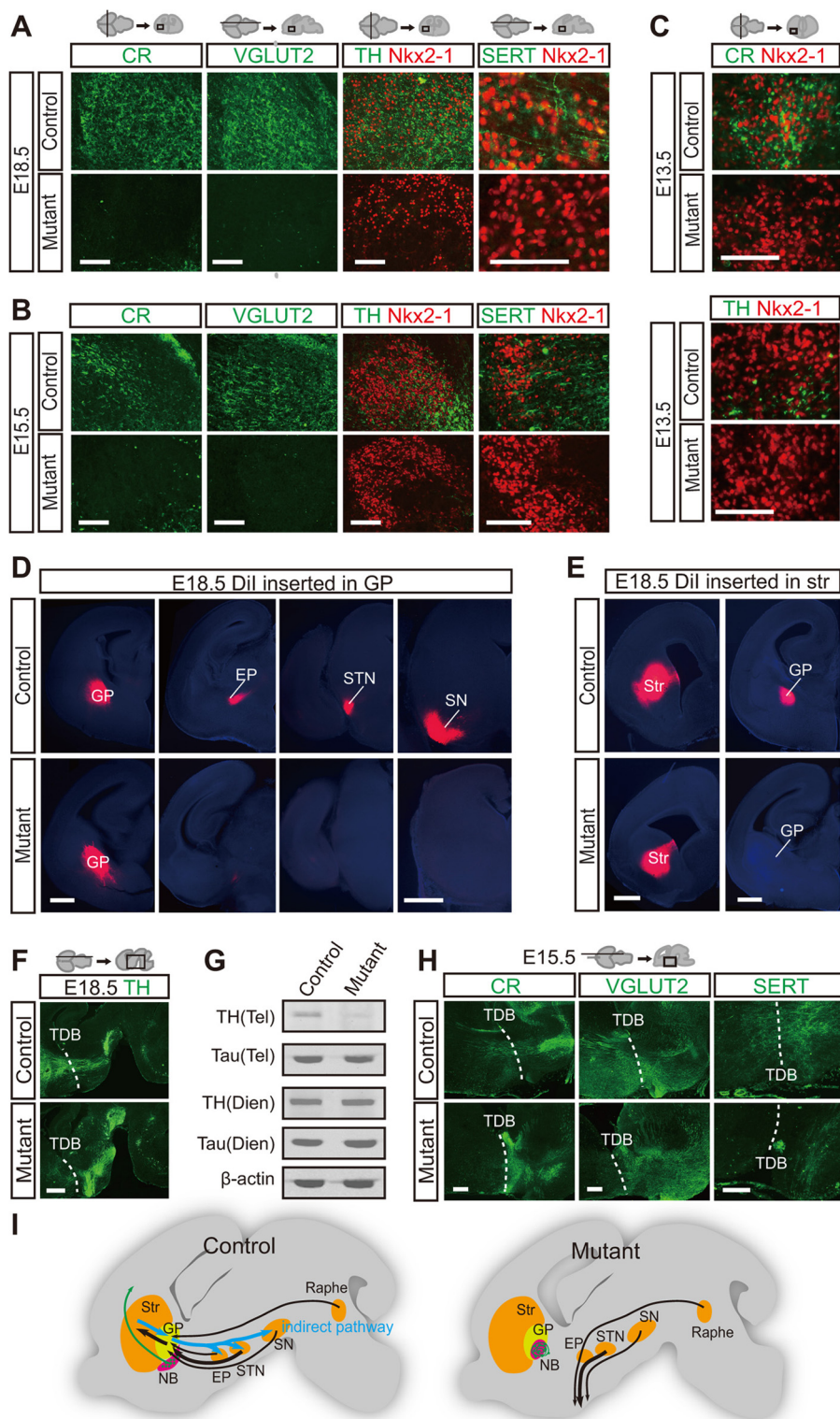


FIG 10 Absence of GP axonal connections in the *Celsr3* mutant. (A and B) CR, VGLUT2, TH, and SERT staining of the mutant and control E18.5 (A) and E15.5 (B) GP. (C) CR and TH staining of the E13.5 GP. (D) Axonal tracing with Dil inserted in the E18.5 GP and observed at caudal levels ($n = 3$ mice). (E) Axonal tracing at E18.5 by inserting Dil in the rostral striatum and sectioning to GP levels ($n = 3$ mice). (F) TH staining of forebrain sagittal sections. (G) Western blot of TH and Tau in the telencephalon and diencephalon with β -actin as a control. (H) CR, VGLUT2, and SERT staining of sagittal sections. (I) Schema depicting the GP axonal connectivity defects. EP, entopeduncular nucleus; STN, subthalamic nucleus; SN, substantia nigra; Dien, diencephalon; Tel, telencephalon; TDB, telencephalon-diencephalon boundary. Scale bars, 100 μ m (A to C), 400 μ m (D to F), and 200 μ m (H).

recent studies identified ~120 diverse membrane-associated proteins, including numerous protocadherins with a conserved WAVE regulatory complex (WRC)-interacting receptor sequence (WIRS) motif that may regulate the actin dynamics during cell migration through the pentamer WRC (69, 71). Interestingly, we found that the *Celsr3* cytoplasmic domain contains a perfect WIRS motif (LASFNS) that may stimulate actin dynamics during cell migration. This is consistent with our previous finding of interneuron migration defects in the *Celsr3* deletion mice (11). Similar defects may occur for the migration of NB cells; in view of the increased apoptosis in GP, we favor the idea that GP structure is altered due to cell loss and the NB simply fills the space left by the dead cells. Strikingly, *Pcdh10* also contains WIRS motifs that stimulate activity of the WRC complex (71). Given the high similarity of the IC cell domain defects in the caudal GP, it is tempting to speculate that both *Celsr3* and *Pcdh10* regulate actin dynamics in the caudal GP at the ventral forebrain through the common downstream WRC complex.

In summary, we found that *Celsr3* is essential for axonal connections between GP and other brain nuclei. Dopaminergic, serotonergic, CR⁺, and glutamatergic axons all have pathfinding defects through the TDB to the GP in the *Celsr3* mutant mice. The defects of GP connectivity cause diverse human diseases (19). *Celsr3* mutant mice may be a useful model for investigating normal GP development and its malfunctions in human neurological diseases.

ACKNOWLEDGMENTS

This work was supported by grants 31171015 and 30970669 from the National Natural Science Foundation of China, 2009CB918701 from the Ministry of Science and Technology of China, and 13XD1402000 and 14JC1403600 from the Science and Technology Commission of Shanghai Municipality.

We thank Ying-hui Fu, Zoltán Molnár, Louis Ptáček, Yuan Wang, Xiaohong Helena Yang, Yuan Zhu, and Yimin Zou for critical reading of the manuscript and Zoltán Molnár for helpful suggestions on Dil tracing experiments.

REFERENCES

- Wu Q, Maniatis T. 2000. Large exons encoding multiple ectodomains are a characteristic feature of protocadherin genes. Proc. Natl. Acad. Sci. U. S. A. 97:3124–3129. <http://dx.doi.org/10.1073/pnas.97.7.3124>.
- Usui T, Shima Y, Shimada Y, Hirano S, Burgess RW, Schwarz TL, Takeichi M, Uemura T. 1999. Flamingo, a seven-pass transmembrane cadherin, regulates planar cell polarity under the control of Frizzled. Cell 98:585–595. [http://dx.doi.org/10.1016/S0092-8674\(00\)80046-X](http://dx.doi.org/10.1016/S0092-8674(00)80046-X).
- Chae J, Kim MJ, Goo JH, Collier S, Gubb D, Charlton J, Adler PN, Park WJ. 1999. The Drosophila tissue polarity gene starry night encodes a member of the protocadherin family. Development 126:5421–5429.
- Gao FB, Kohwi M, Brennan JE, Jan LY, Jan YN. 2000. Control of dendritic field formation in Drosophila: the roles of flamingo and competition between homologous neurons. Neuron 28:91–101. [http://dx.doi.org/10.1016/S0896-6273\(00\)00088-X](http://dx.doi.org/10.1016/S0896-6273(00)00088-X).
- Lee RC, Clandinin TR, Lee CH, Chen PL, Meinertzhagen IA, Zipursky SL. 2003. The protocadherin Flamingo is required for axon target selection in the Drosophila visual system. Nat. Neurosci. 6:557–563. <http://dx.doi.org/10.1038/nn1063>.
- Chen WS, Antic D, Matis M, Logan CY, Povelones M, Anderson GA, Nusse R, Axelrod JD. 2008. Asymmetric homotypic interactions of the atypical cadherin flamingo mediate intercellular polarity signaling. Cell 133:1093–1105. <http://dx.doi.org/10.1016/j.cell.2008.04.048>.
- Matsubara D, Horiuchi SY, Shimono K, Usui T, Uemura T. 2011. The seven-pass transmembrane cadherin Flamingo controls dendritic self-avoidance via its binding to a LIM domain protein, Espinas, in Drosophila sensory neurons. Genes Dev. 25:1982–1996. <http://dx.doi.org/10.1101/gad.16531611>.
- Tissir F, Bar I, Jossin Y, De Backer O, Goffinet AM. 2005. Protocadherin *Celsr3* is crucial in axonal tract development. Nat. Neurosci. 8:451–457. <http://dx.doi.org/10.1038/nn1428>.
- Shima Y, Kawaguchi SY, Kosaka K, Nakayama M, Hoshino M, Nabeshima Y, Hirano T, Uemura T. 2007. Opposing roles in neurite growth control by two seven-pass transmembrane cadherins. Nat. Neurosci. 10:963–969. <http://dx.doi.org/10.1038/nn1933>.
- Zhou L, Bar I, Achouri Y, Campbell K, De Backer O, Hebert JM, Jones K, Kessaris N, de Rouvroit CL, O’Leary D, Richardson WD, Goffinet AM, Tissir F. 2008. Early forebrain wiring: genetic dissection using conditional *Celsr3* mutant mice. Science 320:946–949. <http://dx.doi.org/10.1126/science.1155244>.
- Ying G, Wu S, Hou R, Huang W, Capecchi MR, Wu Q. 2009. The protocadherin gene *Celsr3* is required for interneuron migration in the mouse forebrain. Mol. Cell. Biol. 29:3045–3061. <http://dx.doi.org/10.1128/MCB.00011-09>.
- Fenstermaker AG, Prasad AA, Bechara A, Adolfs Y, Tissir F, Goffinet A, Zou Y, Pasterkamp RJ. 2010. Wnt/planar cell polarity signaling controls the anterior-posterior organization of monoaminergic axons in the brainstem. J. Neurosci. 30:16053–16064. <http://dx.doi.org/10.1523/JNEUROSCI.4508-10.2010>.
- Qu Y, Glasco DM, Zhou L, Sawant A, Ravni A, Fritzsch B, Damrau C, Murdoch JN, Evans S, Pfaff SL, Formstone C, Goffinet AM, Chandrasekhar A, Tissir F. 2010. Atypical cadherins *Celsr1-3* differentially regulate migration of facial branchiomotor neurons in mice. J. Neurosci. 30:9392–9401. <http://dx.doi.org/10.1523/JNEUROSCI.0124-10.2010>.
- Tissir F, Qu Y, Montcouquiol M, Zhou L, Komatsu K, Shi D, Fujimori T, Labbeau J, Tytca D, Courtoy P, Poumay Y, Uemura T, Goffinet AM. 2010. Lack of cadherins *Celsr2* and *Celsr3* impairs ependymal ciliogenesis, leading to fatal hydrocephalus. Nat. Neurosci. 13:700–707. <http://dx.doi.org/10.1038/nn.2555>.
- Lewis A, Wilson N, Stearns G, Johnson N, Nelson R, Brockerhoff SE. 2011. *Celsr3* is required for normal development of GABA circuits in the inner retina. PLoS Genet. 7:e1002239. <http://dx.doi.org/10.1371/journal.pgen.1002239>.
- Feng J, Xu Y, Wang M, Ruan Y, So KF, Tissir F, Goffinet A, Zhou L. 2012. A role for atypical cadherin *celsr3* in hippocampal maturation and connectivity. J. Neurosci. 32:13729–13743. <http://dx.doi.org/10.1523/JNEUROSCI.1965-12.2012>.
- Gerfen CR. 2004. Basal ganglia, p 455–508. In George P (ed), The rat nervous system, 3rd ed. Academic Press, Burlington, MA.
- Mallet N, Micklem BR, Henny P, Brown MT, Williams C, Bolam JP, Nakamura KC, Magill PJ. 2012. Dichotomous organization of the external globus pallidus. Neuron 74:1075–1086. <http://dx.doi.org/10.1016/j.neuron.2012.04.027>.
- Albin RL, Young AB, Penney JB. 1989. The functional anatomy of basal ganglia disorders. Trends Neurosci. 12:366–375. [http://dx.doi.org/10.1016/0166-2236\(89\)90074-X](http://dx.doi.org/10.1016/0166-2236(89)90074-X).
- Gerfen CR. 1992. The neostriatal mosaic: multiple levels of compartmental organization in the basal ganglia. Annu. Rev. Neurosci. 15:285–320. <http://dx.doi.org/10.1146/annurev.ne.15.030192.001441>.
- Nóbrega-Pereira S, Gelman D, Bartolini G, Pla R, Pierani A, Marin O. 2010. Origin and molecular specification of globus pallidus neurons. J. Neurosci. 30:2824–2834. <http://dx.doi.org/10.1523/JNEUROSCI.4023-09.2010>.
- Sussel L, Marin O, Kimura S, Rubenstein JL. 1999. Loss of *Nlx2.1* homeobox gene function results in a ventral to dorsal molecular reSpecification within the basal telencephalon: evidence for a transformation of the pallidum into the striatum. Development 126:3359–3370.
- Flandrin P, Kimura S, Rubenstein JL. 2010. The progenitor zone of the ventral medial ganglionic eminence requires *Nlx2-1* to generate most of the globus pallidus but few neocortical interneurons. J. Neurosci. 30: 2812–2823. <http://dx.doi.org/10.1523/JNEUROSCI.4228-09.2010>.
- Flandrin P, Zhao Y, Vogt D, Jeong J, Long J, Potter G, Westphal H, Rubenstein JL. 2011. *Lhx6* and *Lhx8* coordinately induce neuronal expression of *Shh* that controls the generation of interneuron progenitors. Neuron 70:939–950. <http://dx.doi.org/10.1016/j.neuron.2011.04.020>.
- Métin C, Godement P. 1996. The ganglionic eminence may be an intermediate target for corticofugal and thalamocortical axons. J. Neurosci. 16:3219–3235.
- Molnár Z, Adams R, Blakemore C. 1998. Mechanisms underlying the early establishment of thalamocortical connections in the rat. J. Neurosci. 18:5723–5745.

27. Tuttle R, Nakagawa Y, Johnson JE, O'Leary DD. 1999. Defects in thalamocortical axon pathfinding correlate with altered cell domains in Mash-1-deficient mice. *Development* 126:1903–1916.
28. Uemura M, Nakao S, Suzuki ST, Takeichi M, Hirano S. 2007. OL-protocadherin is essential for growth of striatal axons and thalamocortical projections. *Nat. Neurosci.* 10:1151–1159. <http://dx.doi.org/10.1038/nn1960>.
29. Molnár Z, Garel S, López-Bendito G, Maness P, Price DJ. 2012. Mechanisms controlling the guidance of thalamocortical axons through the embryonic forebrain. *Eur. J. Neurosci.* 35:1573–1585. <http://dx.doi.org/10.1111/j.1460-9568.2012.08119.x>.
30. Guo Y, Monahan K, Wu H, Gertz J, Varley KE, Li W, Myers RM, Maniatis T, Wu Q. 2012. CTCF/cohesin-mediated DNA looping is required for protocadherin alpha promoter choice. *Proc. Natl. Acad. Sci. U. S. A.* 109:21081–21086. <http://dx.doi.org/10.1073/pnas.1219280110>.
31. Splinter E, de Wit E, van de Werken HJ, Klous P, de Laat W. 2012. Determining long-range chromatin interactions for selected genomic sites using 4C-seq technology: from fixation to computation. *Methods* 58:221–230. <http://dx.doi.org/10.1016/j.ymeth.2012.04.009>.
32. Thongjuea S, Stadhouders R, Grosveld FG, Soler E, Lenhard B. 2013. r3Cseq: an R/Bioconductor package for the discovery of long-range genomic interactions from chromosome conformation capture and next-generation sequencing data. *Nucleic Acids Res.* 41:e132. <http://dx.doi.org/10.1093/nar/gkt373>.
33. Langmead B, Trapnell C, Pop M, Salzberg SL. 2009. Ultrafast and memory-efficient alignment of short DNA sequences to the human genome. *Genome Biol.* 10:R25. <http://dx.doi.org/10.1186/gb-2009-10-3-r25>.
34. Zhang Y, Liu T, Meyer CA, Eeckhout J, Johnson DS, Bernstein BE, Nusbaum C, Myers RM, Brown M, Li W, Liu XS. 2008. Model-based analysis of ChIP-Seq (MACS). *Genome Biol.* 9:R137. <http://dx.doi.org/10.1186/gb-2008-9-9-r137>.
35. Hedreen JC, Bacon SJ, Price DL. 1985. A modified histochemical technique to visualize acetylcholinesterase-containing axons. *J. Histochem. Cytochem.* 33:134–140. <http://dx.doi.org/10.1177/33.2.2578498>.
36. Saito T, Nakatsuji N. 2001. Efficient gene transfer into the embryonic mouse brain using in vivo electroporation. *Dev. Biol.* 240:237–246. <http://dx.doi.org/10.1006/dbio.2001.0439>.
37. Tissir F, De-Backer O, Goffinet AM, Lambert de Rouvroit C. 2002. Developmental expression profiles of Celsr (Flamingo) genes in the mouse. *Mech. Dev.* 112:157–160. [http://dx.doi.org/10.1016/S0925-4773\(01\)00623-2](http://dx.doi.org/10.1016/S0925-4773(01)00623-2).
38. Kehayova P, Monahan K, Chen W, Maniatis T. 2011. Regulatory elements required for the activation and repression of the protocadherin-alpha gene cluster. *Proc. Natl. Acad. Sci. U. S. A.* 108:17195–17200. <http://dx.doi.org/10.1073/pnas.1114357108>.
39. Johnson DS, Mortazavi A, Myers RM, Wold B. 2007. Genome-wide mapping of in vivo protein-DNA interactions. *Science* 316:1497–1502. <http://dx.doi.org/10.1126/science.1141319>.
40. Zhao Y, Marín O, Hermes E, Powell A, Flames N, Palkovits M, Rubenstein JL, Westphal H. 2003. The LIM-homeobox gene Lhx8 is required for the development of many cholinergic neurons in the mouse forebrain. *Proc. Natl. Acad. Sci. U. S. A.* 100:9005–9010. <http://dx.doi.org/10.1073/pnas.1537759100>.
41. Elshatory Y, Gan L. 2008. The LIM-homeobox gene Islet-1 is required for the development of restricted forebrain cholinergic neurons. *J. Neurosci.* 28:3291–3297. <http://dx.doi.org/10.1523/JNEUROSCI.5730-07.2008>.
42. López-Bendito G, Cautinat A, Sanchez JA, Bielle F, Flames N, Garratt AN, Talmage DA, Role LW, Charnay P, Marín O, Garel S. 2006. Tangential neuronal migration controls axon guidance: a role for neuroligin-1 in thalamocortical axon navigation. *Cell* 125:127–142. <http://dx.doi.org/10.1016/j.cell.2006.01.042>.
43. Côté PY, Parent A. 1992. Calbindin D-28k and choline acetyltransferase are expressed by different neuronal populations in pedunculopontine nucleus but not in nucleus basalis in squirrel monkeys. *Brain Res.* 593:245–252.
44. Molnár Z, Higashi S, López-Bendito G. 2003. Choreography of early thalamocortical development. *Cereb. Cortex* 13:661–669. <http://dx.doi.org/10.1093/cercor/13.6.661>.
45. Molnár Z, Cordery P. 1999. Connections between cells of the internal capsule, thalamus, and cerebral cortex in embryonic rat. *J. Comp. Neurol.* 413:1–25. [http://dx.doi.org/10.1002/\(SICI\)1096-9861\(19991011\)413:1<1::AID-CNE1>3.0.CO;2-5](http://dx.doi.org/10.1002/(SICI)1096-9861(19991011)413:1<1::AID-CNE1>3.0.CO;2-5).
46. Lakhina V, Falnikar A, Bhatnagar L, Tole S. 2007. Early thalamocortical tract guidance and topographic sorting of thalamic projections requires LIM-homeodomain gene Lhx2. *Dev. Biol.* 306:703–713. <http://dx.doi.org/10.1016/j.ydbio.2007.04.007>.
47. Alexander GE, Crutcher MD. 1990. Functional architecture of basal ganglia circuits: neural substrates of parallel processing. *Trends Neurosci.* 13:266–271. [http://dx.doi.org/10.1016/0166-2236\(90\)90107-L](http://dx.doi.org/10.1016/0166-2236(90)90107-L).
48. Kita H. 2007. Globus pallidus external segment. *Prog. Brain Res.* 160:111–133. [http://dx.doi.org/10.1016/S0079-6123\(06\)60007-1](http://dx.doi.org/10.1016/S0079-6123(06)60007-1).
49. Halbleib JM, Nelson WJ. 2006. Cadherins in development: cell adhesion, sorting, and tissue morphogenesis. *Genes Dev.* 20:3199–3214. <http://dx.doi.org/10.1101/gad.1486806>.
50. Chen WV, Maniatis T. 2013. Clustered protocadherins. *Development* 140:3297–3302. <http://dx.doi.org/10.1242/dev.090621>.
51. Wu Q, Maniatis T. 1999. A striking organization of a large family of human neural cadherin-like cell adhesion genes. *Cell* 97:779–790. [http://dx.doi.org/10.1016/S0092-8674\(00\)80789-8](http://dx.doi.org/10.1016/S0092-8674(00)80789-8).
52. Tasic B, Nabholz CE, Baldwin KK, Kim Y, Rueckert EH, Ribich SA, Cramer P, Wu Q, Axel R, Maniatis T. 2002. Promoter choice determines splice site selection in protocadherin alpha and gamma pre-mRNA splicing. *Mol. Cell* 10:21–33. [http://dx.doi.org/10.1016/S1097-2765\(02\)00578-6](http://dx.doi.org/10.1016/S1097-2765(02)00578-6).
53. Wang X, Su H, Bradley A. 2002. Molecular mechanisms governing Pcdh-gamma gene expression: evidence for a multiple promoter and cis-alternative splicing model. *Genes Dev.* 16:1890–1905. <http://dx.doi.org/10.1101/gad.1004802>.
54. Tan YP, Li S, Jiang XJ, Loh W, Foo YK, Loh CB, Xu Q, Yuen WH, Jones M, Fu J, Venkatesh B, Yu WP. 2010. Regulation of protocadherin gene expression by multiple neuron-restrictive silencer elements scattered in the gene cluster. *Nucleic Acids Res.* 38:4985–4997. <http://dx.doi.org/10.1093/nar/gkq246>.
55. Hirayama T, Tarusawa E, Yoshimura Y, Galjart N, Yagi T. 2012. CTCF is required for neural development and stochastic expression of clustered Pcdh genes in neurons. *Cell Rep.* 2:345–357. <http://dx.doi.org/10.1016/j.celrep.2012.06.014>.
56. Handoko L, Xu H, Li G, Ngan CY, Chew E, Schnapp M, Lee CW, Ye C, Ping JL, Mulawadi F, Wong E, Sheng J, Zhang Y, Poh T, Chan CS, Kunarso G, Shahab A, Bourque G, Cacheux-Rataboul V, Sung WK, Ruan Y, Wei CL. 2011. CTCF-mediated functional chromatin interactome in pluripotent cells. *Nat. Genet.* 43:630–638. <http://dx.doi.org/10.1038/ng.857>.
57. Dixon JR, Selvaraj S, Yue F, Kim A, Li Y, Shen Y, Hu M, Liu JS, Ren B. 2012. Topological domains in mammalian genomes identified by analysis of chromatin interactions. *Nature* 485:376–380. <http://dx.doi.org/10.1038/nature11082>.
58. Xu Q, Tam M, Anderson SA. 2008. Fate mapping Nkx2.1-lineage cells in the mouse telencephalon. *J. Comp. Neurol.* 506:16–29. <http://dx.doi.org/10.1002/cne.21529>.
59. Pombero A, Bueno C, Saglietti L, Rodenas M, Guimera J, Bulfone A, Martinez S. 2011. Pallial origin of basal forebrain cholinergic neurons in the nucleus basalis of Meynert and horizontal limb of the diagonal band nucleus. *Development* 138:4315–4326. <http://dx.doi.org/10.1242/dev.069534>.
60. Mesulam MM, Mufson EJ, Wainer BH, Levey AI. 1983. Central cholinergic pathways in the rat: an overview based on an alternative nomenclature (Ch1-Ch6). *Neuroscience* 10:1185–1201. [http://dx.doi.org/10.1016/0306-4522\(83\)90108-2](http://dx.doi.org/10.1016/0306-4522(83)90108-2).
61. Bohnen NI, Albin RL. 2011. The cholinergic system and Parkinson disease. *Behav. Brain Res.* 221:564–573. <http://dx.doi.org/10.1016/j.bbr.2009.12.048>.
62. López-Bendito G, Molnár Z. 2003. Thalamocortical development: how are we going to get there? *Nat. Rev. Neurosci.* 4:276–289. <http://dx.doi.org/10.1038/nrn1075>.
63. Zhou L, Qu Y, Tissir F, Goffinet AM. 2009. Role of the atypical cadherin Celsr3 during development of the internal capsule. *Cereb. Cortex* 19(Suppl 1):i114–119. <http://dx.doi.org/10.1093/cercor/bhp032>.
64. Marín O, Baker J, Puelles L, Rubenstein JL. 2002. Patterning of the basal telencephalon and hypothalamus is essential for guidance of cortical projections. *Development* 129:761–773.
65. Schreiner D, Weiner JA. 2010. Combinatorial homophilic interaction between gamma-protocadherin multimers greatly expands the molecular diversity of cell adhesion. *Proc. Natl. Acad. Sci. U. S. A.* 107:14893–14898. <http://dx.doi.org/10.1073/pnas.1004526107>.
66. Suo L, Lu HN, Ying GX, Capecchi MR, Wu Q. 2012. Protocadherin clusters and cell adhesion kinase regulate dendrite complexity through Rho GTPase. *J. Mol. Cell Biol.* 4:362–376. <http://dx.doi.org/10.1093/jmcb/mjs034>.

67. Lefebvre JL, Kostadinov D, Chen WV, Maniatis T, Sanes JR. 2012. Protocadherins mediate dendritic self-avoidance in the mammalian nervous system. *Nature* 488:517–521. <http://dx.doi.org/10.1038/nature11305>.
68. Prasad T, Weiner JA. 2011. Direct and indirect regulation of spinal cord Ia afferent terminal formation by the gamma-protocadherins. *Front. Mol. Neurosci.* 4:54. <http://dx.doi.org/10.3389/fnmol.2011.00054>.
69. Biswas S, Emond MR, Duy PQ, Hao le T, Beattie CE, Jontes JD. 2014. Protocadherin-18b interacts with Nap1 to control motor axon growth and arborization in zebrafish. *Mol. Biol. Cell* 25:633–642. <http://dx.doi.org/10.1091/mbc.E13-08-0475>.
70. Hoshina N, Tanimura A, Yamasaki M, Inoue T, Fukabori R, Kuroda T, Yokoyama K, Tezuka T, Sagara H, Hirano S, Kiyonari H, Takada M, Kobayashi K, Watanabe M, Kano M, Nakazawa T, Yamamoto T. 2013. Protocadherin 17 regulates presynaptic assembly in topographic cortico-basal ganglia circuits. *Neuron* 78:839–854. <http://dx.doi.org/10.1016/j.neuron.2013.03.031>.
71. Chen BY, Brinkmann K, Chen ZC, Pak CW, Liao YX, Shi SY, Henry L, Grishin NV, Bogdan S, Rosen MK. 2014. The WAVE regulatory complex links diverse receptors to the actin cytoskeleton. *Cell* 156:195–207. <http://dx.doi.org/10.1016/j.cell.2013.11.048>.